# The Role of Maternal HP1a in Early *Drosophila* Embryogenesis via Regulation of Maternal Transcript Production

**Ah Rume Park,*,†,1 Na Liu,*,†,1 Nils Neuenkirchen,*,† Qiaozhi Guo,*,† and Haifan Lin*,†,2**
*Yale Stem Cell Center and †Department of Cell Biology, Yale University School of Medicine, New Haven, Connecticut 06520

**ABSTRACT** Heterochromatin protein 1a (HP1a) is a highly conserved and versatile epigenetic factor that can both silence and activate transcription. However, the function of HP1a in development has been underinvestigated. Here, we report the role of maternal HP1a in producing maternal transcripts that drive early *Drosophila* embryogenesis. Maternal HP1a upregulates genes involved in translation, mRNA splicing, and cell division, but downregulates genes involved in neurogenesis, organogenesis, and germline development, which all occur later in development. Our study reveals the earliest contribution of HP1a during oogenesis in regulating the production of maternal transcripts that drive early *Drosophila* embryogenesis.

**KEYWORDS** HP1a; maternal transcriptome; embryonic mitosis; oogenesis

HETEROCHROMATIN protein 1a (HP1a) is a nonhistone chromosomal protein that was first discovered in the heterochromatin of *Drosophila melanogaster* (James and Elgin 1986). HP1a is highly conserved during evolution and predominantly localizes to heterochromatin to induce gene silencing (James and Elgin 1986). In *Drosophila*, HP1a is encoded by the *Su(var)2-5* gene, first discovered for its dosage-dependent effect on position-effect variegation (Muller and Tyler 1930; Elgin and Reuter 2013). HP1a contains two conserved domains. The chromo domain, residing in the N-terminal half of the protein, is responsible for interacting with chromatin through binding to methylated lysine 9 of histone 3 (H3K9me3) to form compact chromatin (Bannister *et al.* 2001). The chromo shadow domain, residing in the C-terminal half of the protein, is required for HP1 dimerization and interaction with other proteins by binding to a conserved PxVxL motif in these proteins (Li *et al.* 2003). The role of HP1a in heterochromatin formation and epigenetic gene silencing in diverse species has been described by the following model: histone methyltransferases methylate the H3K9me marks, creating binding sites for the chromo domain of HP1a (Paro and Hogness 1991). Once bound to chromatin, HP1a recruits a histone methyltransferase, which methylates adjacent H3K9, creating more binding sites for HP1a. Subsequent dimerization of nearby HP1a via the chromo shadow domain leads to a higher-order chromatin state that represses gene expression and the spreading of heterochromatin (Lachner *et al.* 2001).

Emerging evidence indicates that HP1a also positively regulates euchromatic gene expression (Piacentini *et al.* 2003). HP1a was shown to associate with euchromatic sites on the polytene chromosomes of *Drosophila* using an anti-HP1a antibody (Richards and Elgin 2002), as well as in mapping via Dam-ID (Greil *et al.* 2003) and HP1a chromatin immunoprecipitation-sequencing (ChIP-seq) (Fleming *et al.* 2011). HP1a colocalizes with the active form of RNA polymerase (pol) II, which also co-immunoprecipitates with HP1a, at multiple euchromatic sites in the polytene chromosome (James *et al.* 1989). HP1a ChIP-seq data revealed that it localizes to transcription start sites of highly expressed genes in adult flies. HP1a enrichment in promoter regions mimics that of RNA pol II, suggesting that HP1a may function together with RNA pol II in transcription activation (Yin *et al.* 2011). Furthermore, expression of euchromatic genes, some of which were shown to be associated with HP1a, was downregulated in HP1a-deficient *Drosophila* larvae (Cryderman *et al.* 2005) and in a cultured *Drosophila* embryonic cell line (De Lucia *et al.* 2005). HP1a was shown to positively regulate


doi: https://doi.org/10.1534/genetics.118.301704
Manuscript received May 19, 2018; accepted for publication November 7, 2018; published Early Online November 15, 2018.
Supplemental material available at Figshare: https://doi.org/10.25386/genetics.7263251.
[1]These authors contributed equally to this work.
[2]Corresponding author: Room 237, 10 Amistad, Yale University School of Medicine, New Haven, CT 06519. E-mail: haifan.lin@yale.edu

euchromatic gene expression through interaction with RNA transcripts and heterogeneous nuclear ribonucleoproteins (hnRNPs) that participate in RNA processing and heterochromatin formation (Piacentini *et al.* 2009).

Moreover, HP1a plays a critical role during cell division, which is a major event of early development. Kellum and Alberts showed various chromosomal segregation defects in embryos from heterozygous HP1a mutant female flies and attributed this to the involvement of HP1a in chromatin organization (Kellum and Alberts 1995). They demonstrated a dose-dependent effect of maternal HP1a in chromosome segregation during early cycles of *Drosophila* embryogenesis. The authors have also shown that a large portion of the HP1a population is dissociated with the segregating chromosomes and dispersed around them during cell division (Kellum *et al.* 1995), confirming the direct participation of HP1a in mitosis. Hirota *et al.* later showed that Aurora B mediates the dissociation of the HP1 protein from heterochromatin by phosphorylating H3 on serine 10 during mitosis (Hirota *et al.* 2005).

Although a direct role of HP1a in cell division has been proposed, this role may not be fully accountable for the early embryonic function of HP1a, since HP1a may also regulate the transcription of the maternal transcripts during oogenesis, which in turn would have an important impact on many events during early embryogenesis. In mammals and invertebrates alike, maternal gene products regulate all aspects of early development, including fertilization, the completion of meiosis, initiation of embryonic mitotic cell cycles, embryonic patterning, and activation of the zygotic genome (Marlow 2010). In *Drosophila*, maternal transcripts that are made in nurse cells in the ovary are passed onto the oocyte around oogenic stage 10 via a process called nurse cell dumping (Gutzeit and Koppa 1982). These maternal products drive the early embryogenesis until (and after) bulk zygotic transcription takes place during maternal-to-zygotic transition at embryonic cycle 14 (Edgar and Schubiger 1986). Thus, in this study, we investigate the function of HP1a during oogenesis in regulating the production of the maternal transcriptome and the effect of this regulation in early embryogenesis. Our results revealed a broader impact of transcriptional regulation by maternal HP1a that drives early *Drosophila* development.

## Materials and Methods

### *Drosophila stocks*

All *Drosophila* stocks were raised on standard agar/molasses medium at 25°. The $w^{1118}$ strain served as the wild-type control. For RNA interference (RNAi)-induced knockdown of *Su(var)2-5*, a Transgenic RNAi Project (TRiP) fly generated using short hairpin HMS00278 (#33400; RNAi #1; Bloomington *Drosophila* Stock Center) and a second transgenic HP1a short hairpin RNA (shRNA) fly generated using the φC31 method in this study (Supplemental Material; RNAi #2) was used to address off-target effects. Corresponding enhanced GFP (EGFP) shRNA controls (#41556 and #41558, respectively; Bloomington *Drosophila* Stock Center) were used to address position-effect variation. All RNAi lines were driven by maternal α-tubulin GAL4 (#7062; Bloomington *Drosophila* Stock Center) or MTD-GAL4 (Petrella *et al.* 2007). To characterize HP1a expression and to label the paternal zygotic copy of HP1a, an EGFP-HP1a knock-in line was generated using clustered regularly interspaced short palindromic repeat (CRISPR)/Cas9 technology in this study (Supplemental Material) and a transgenic GFP-HP1a line with an insertion on the third chromosome (#30561; Bloomington *Drosophila* Stock Center) was used as a positive control. A *Su(var)2-5$^{04}$/CyO·GFP* mutant allele was used (Eissenberg *et al.* 1992).

### *Immunofluorescence microscopy of the ovary*

Ovaries were dissected from 2- to 3-day-old adult female flies in ice-cold phosphate buffered saline (PBS), and were fixed for 20 min in fixative (0.5% NP40 and 2% formaldehyde in PBS) at room temperature. After washing in PBST (PBS + 0.1% Triton X-100), ovaries were stained with DAPI (1:1000) and mounted in Vectashield (Vector Laboratories, Burlingame, CA). Samples were imaged using a Leica TCS SP5 Spectral Confocal Microscope on sequential scanning mode. Image collection was carried out using the Leica Application Suite imaging software.

### *Egg laying and hatching quantification*

Fifteen females of the indicated genotype ($w^{1118}$, *Su(var)2-5$^{04}$/CyO·GFP*, *Su(var)2-5$^{04}$/+* ; *HP1a* RNAi #1, *Su(var)2-5$^{04}$/+* ; *HP1a* RNAi #2, *Su(var)2-5$^{04}$/+* ; *EGFP* RNAi #1, or *Su(var)2-5$^{04}$/+* ; *EGFP* RNAi #2) were placed with five $w^{1118}$ males in small embryo collection cages and allowed to lay eggs on grape juice agar plates with yeast paste at 25°. To assess fertility, plates were removed at days 2, 4, 6, 8, 10, and 12, and the number of eggs laid was counted. For egg-hatching rates, the same plates were sealed with parafilm and incubated at 25° for 30 hr to ensure enough time for all eggs to be hatched. The number of eggs that were hatched after the 30-hr incubation were counted and the percentage of the hatching rate was calculated. The number of eggs laid and percent hatch rate represent the mean from three independent embryo collections.

### *Immunoblotting*

Protein samples from stage 14 eggs or ovaries were heat-denatured in 6× SDS Sample Buffer, resolved on Mini-Protean TGX precast Gels (Bio-Rad, Hercules, CA), transferred to a nitrocellulose membrane, and detected with the appropriate HRP-conjugated anti-mouse or anti-rabbit secondary antibody (1:5000; Jackson Labs) and Clarity Western ECL Substrate (Bio-Rad). The following primary antibodies were used at the indicated dilutions: monoclonal mouse anti-HP1a (1:25; C1A9 Developmental Studies Hybridoma Bank), rabbit anti-H4Ac, rabbit anti-H3K9me3, mouse anti-H3K27me3, rabbit anti-H3K4me3, rabbit anti-H2Av, and GAPDH (1:2000).

### Detection of paternal zygotic HP1a

Wild-type ($w^{1118}$) females and EGFP-HP1a knock-in males (generated using the CRISPR/Cas9 method, Supplemental Material) were crossed to selectively label the paternal zygotic allele of HP1a in the F1 embryos. Next, 0–2 hr embryos fixed in methanol (MeOH) and stained in DAPI were individually placed in 50% glycerol and 50% PBS solution in each well of a 96-well plate. Each embryo was visualized and staged under an inverted fluorescent microscope (Su 2007). Five embryos of the same stage were collected for each of mitotic cycles 11–14 for transcript (Figure 2B) or protein (Figure 2C) detection. For transcript detection, RNA was extracted from five embryos of the same stage using an RNeasy Micro Kit (QIAGEN, Valencia, CA) and reverse transcribed using High-Capacity cDNA Reverse Transcription Kit (Applied Biosystems, Foster City, CA). GFP-HP1a transcript was detected via PCR amplification using the following primers: EGFP_FOR, 5′-GACGTAAACGGCCACAAGTTCAGCG-3′ and HP1a_REV, 5′-CCTGCTCCGCATCTGTGGTACG-3'. The primers were designed so that the amplified complementary DNA is distinguished from the longer genomic DNA. For GFP-HP1a protein detection, five embryos of the same stage were incubated in 6× SDS Sample Buffer for 8 min at 95°. GFP-HP1a was detected in an immunoblot using mouse anti-HP1a (1:25; C1A9 Developmental Studies Hybridoma Bank) as the ∼50 kDa band (untagged HP1a is detected at ∼24 kDa).

### Embryo fixation and immunostaining

Embryos were collected in small embryo collection cages on grape juice agar plates, and dechorionated in 50% bleach for 2 min and thoroughly washed. The embryos were then fixed in 50% heptane and 50% fixative (three parts 1.33× PBS and 67 mM EGTA: one part 37% formaldehyde) for 10 min at room temperature. After removing the fixative, ice-cold MeOH was added and embryos were vortexed for 1 min to remove the vitelline membrane. Embryos were washed in MeOH three times, and either stored at −20° for future use or immediately rehydrated in an MeOH:PBST series consisting of 70% MeOH and 30% PBST, 50% MeOH and 50% PBST, 30% MeOH and 70% PBST, and finally 100% PBST for 5 min each on ice. The embryos were blocked in 5% normal goat serum in PBST overnight at 4°.

The following antisera were used for immunofluorescent staining: rabbit α-tubulin antibody (1:200; Abcam), rabbit centrosomin antiserum (1:200, gift from T. Kaufman), mouse monoclonal lamin antibody (1:200; Iowa Hybridoma Bank), rabbit Ser10 phospho histone H3 (PH3) (1:200; Cell Signaling Technology), mouse monoclonal HP1a antibody (1:200; C1A9; Developmental Studies Hybridoma Bank), and rabbit H3K9me3, (1:200; Upstate Biotechnology Co.). All fluorescence-conjugated secondary antibodies were Alexa-Fluor from Invitrogen (Carlsbad, CA) and were used at 1:400 dilution. All dilutions were made in 5% normal goat serum in PBST. After washing in PBST, embryos were stained with DAPI (1:1000), and mounted in Vectashield (Vector Laboratories). Samples were imaged using either a Leica TCS SP5 Spectral Confocal Microscope on sequential scanning mode or a Zeiss (Carl Zeiss, Thornwood, NY) fluorescence microscope. Image collection was carried out using the Leica Application Suite or Zeiss AxioVision imaging software.

### Maternal transcriptome analysis

mRNA sequencing data were collected from a HiSeq2000 at the Yale Stem Cell Center Genomics Core for HP1a RNAi and EGFP RNAi lines, either from stage 14 eggs or ovaries. After the sequencing quality evaluation by FASTQC, sequences were mapped to *D. melanogaster* Berkeley Drosophila Genome Project (BDGP) release 6 by Tophat2.1.1 with the default mapping option (Supplemental Material, Table S1). The gene annotation used for the analysis was *D. melanogaster* BDGP6.84. The Rsubread package was used for the read count assignment (Liao *et al.* 2013). Reproducibility evaluation was measured by Pearson correlation between replicates and visualized in scatterplots (Figure S1, A–D). The schematic of the transcriptome analysis pipeline is displayed in Figure S2A. DEseq2 was applied to analyze the expression level changes of genes in HP1a RNAi samples compared to those of control RNAi samples (Anders and Huber 2010). For each RNAi line, genes with $P$-value $\leq 0.05$ were considered to be differentially expressed (DE) genes. To rule out the effect caused by the different insertion sites of RNAi, we subtracted the differentially expressed genes identified in the control RNAi in the corresponding HP1a RNAi. To account for shRNA off-target effects, we only kept the common differentially expressed genes of the two RNAi lines and regarded those with consistent changes in trend (up- or downregulated) as differentially expressed genes for further analysis. A volcano plot showing the fold change and $P$-value was used to display the mRNA level change for all genes in the HP1a RNAi samples (Figure S1, E and F).

### Gene ontology analysis

For functional enrichment analysis, identified differentially expressed genes were analyzed by the web-based Functional Annotation Tool of Database for Annotation, Visualization and Interated Discovery v6.8: http://david.abcc.ncifcrf.gov/; (Huang da *et al.* 2009).

### Significance analysis for candidate HP1a direct target genes

We randomly picked 1359 genes from the *Drosophila* dm6 genome and calculated the number of genes that contain 2900 HP1a-binding sites. We repeated such a procedure 100,000 times, and the chance of getting 43.3% of genes overlapping with HP1a-binding sites was obtained for the $P$-value, which was $< 0.00001$.

### ChIP

The dissected fly ovaries were homogenized in sucrose buffer AS [60 mM KCl, 15 mM NaCl, 1 mM EDTA (pH 8.0), 0.1 mM

EGTA, 15 mM HEPES (pH 7.4), 0.3 M sucrose, and 1× Protease Inhibitor Cocktail] in a 1.5-ml tube using a plastic homogenizer. The homogenized lysate was subjected to 1% formaldehyde cross-linking at room temperature for 15 min, and then was quenched in 0.125 M glycine at room temperature for 5 min, followed by three 5-min washes in PBST (0.1% Triton X-100 in PBS). Cross-linked nuclei were resuspended in nuclear lysis buffer [10 mM EDTA, 0.5% (w/v) N-lauroylsarcosine, and 50 mM HEPES, pH 8.0] and sonicated using an S-series Covaris sonicator for 9 min to yield fragments that were 200–250-bp long (Figure S3) at a high cell setting. The sonicated lysate was spun down at 14,000 rpm for 20 min at 4° and clear supernatant was used for subsequent immunoprecipitation. Next, 1% of input was stored at −20° for subsequent analyses and rest of the lysate was incubated with 1:200 polyclonal rabbit-anti HP1a antibody (Covance) at 4° overnight. A control rabbit-FLAG (Sigma [Sigma Chemical], St. Louis, MO) immunoprecipitation experiment was conducted in parallel. Salmon sperm DNA-coated Protein A/G magnetic beads (Invitrogen) were added to the sample and were incubated at 4° for 3 hr. After washing four times with radioimmunoprecipitation assay (RIPA) buffer [140 mM NaCl, 1 mM EDTA, 1% Triton X-100 (v/v), 0.1% SDS (w/v), 0.1% sodium deoxycholate (w/v), and 10 mM Tris-HCl, pH 8.0], two times with RIPA 500 buffer [500 mM NaCl, 1 mM EDTA, 1% Triton X-100 (v/v), 0.1% SDS (w/v), 0.1% sodium deoxycholate (w/v), 10 mM Tris-HCl, pH 8.0], two times with lithium chloride buffer [250 mM LiCl, 1 mM EDTA, 0.5% IGEPAL CA-630 (v/v), 0.5% sodium deoxycholate (w/v), and 10 mM Tris-HCl, pH 8.0], and once with Tris EDTA buffer (1 mM EDTA and 10 mM Tris-HCl, pH 8.0), beads were spun at 300 × *g* for 1 min to remove the Tris EDTA buffer. Next, 220 μl of elution buffer (0.1 M $NaHCO_3$ and 1% SDS) was added to each HP1a ChIP, mock FLAG ChIP, and 1% input samples, and DNA–protein was eluted at 65° for 1 hr while shaking on a thermocycler at 1300 rpm. The eluted samples were reverse cross-linked at 65° for 14 hr while shaking on a thermocycler at 1000 rpm. The reverse cross-linked samples were treated with DNase-free RNase A (10 μg/ml; Ambion) at 37° for 1 hr, followed by incubation with Proteinase K (catalog number 745723; Roche) at 55° for 1 hr. DNA was purified for subsequent quantitative PCRs (qPCRs) using the QIAGEN PCR purification kit.

### *Bioinformatic analysis of ovarian HP1a ChIP-seq data*

HP1a ChIP data for three biological replicates were collected from HiSeq2000 at the Yale Stem Cell Center Genomics Core. After the sequencing quality was evaluated by FASTQC, sequences were mapped to *D. melanogaster* BDGP release 6 by Bowtie2 with a default mapping option, where only unique mapping was recorded. Mismatches were not allowed for peak calling. To identify HP1a-binding sites, SICER for ChIP-seq data analysis was applied to each pair of biological replicates with the default option, where the false discovery rate was ≤ 0.05 (a schematic of the pipeline is shown in Figure S2B). In ChIP-seq replicate 1, 3585 regions were identified as HP1a-binding sites, 2914 regions in replicate 2, and 3600 regions in replicate 3. Peaks that were identified in at least two biological replicates were considered to be HP1a-binding sites and used for further analysis. HP1a-binding sites were displayed in a chromosome-based Circos plot for genome-wide visualization (Krzywinski *et al.* 2009). Genes that are within 1 kb of ChIP-binding sites were classified to be HP1a-bound genes.

For all HP1a-bound genes, ChIP-seq signals (reads per million) within 1-kb regions surrounding transcription start sites (TSSs) and transcription termination sites (TTSs) were calculated and plotted with metagene package in R at 20-bp resolution. A total of 11,240 transcripts were aligned. The annotation of HP1a-binding sites was obtained using the RepeatMasker program (http://www.repeatmasker.org) and gene annotation of BDGP release 6.

### *ChIP-qPCR and RT- qPCR*

Genomic DNA fragments purified by HP1a ChIP were used as templates in the qPCR on a Bio-Rad CFX96 real-time PCR machine. For each qPCR, the percentage of HP1a ChIP-DNA and FLAG mock ChIP-DNA as a percentage of the input was calculated using the $2^{-\Delta\Delta CT}$ method.

RT-qPCR was conducted to measure and confirm the transcription activity detected from RNA-seq (RNA-sequencing). Total RNA was extracted from stage 14 eggs using the QIAGEN RNeasy Micro Kit and cDNA libraries were prepared using a High-Capacity cDNA Reverse Transcription Kit (Thermo Fisher Scientific). The cDNA libraries were subjected to qPCR. Primers were from existing literature (De Lucia *et al.* 2005; Huang *et al.* 2013; Xie *et al.* 2016) or designed against exon regions of genes of interest using a *Drosophila* BLAST search using the August 2014 BDGP Release 6 + ISO1 MT/dm6. Each designed primer set was tested on the wild-type stage 14 cDNA to determine the amplification efficiency.

### *Data availability*

All strains and plasmids are available upon request. ChIP and RNA-seq sequence data are available at the National Center for Biotechnology Information database with the accession number PRJNA486847. Supplemental material available at Figshare: https://doi.org/10.25386/genetics.7263251.

## Results

### *HP1a reduction during mid- and late-stage oogenesis leads to defects in ovarian morphology and subfertility*

To investigate the various functions of HP1a during oogenesis, we reduced HP1a expression in the ovary using short-hairpin-induced RNA interference (RNAi). Two shRNA lines against HP1a, referred to as HP1a RNAi #1 and #2 in this study, were used to rule out off-target effects of either RNAi line. HP1a RNAi #1 was obtained from the TRiP (Perkins *et al.* 2015) and HP1a RNAi #2 was newly generated in this study

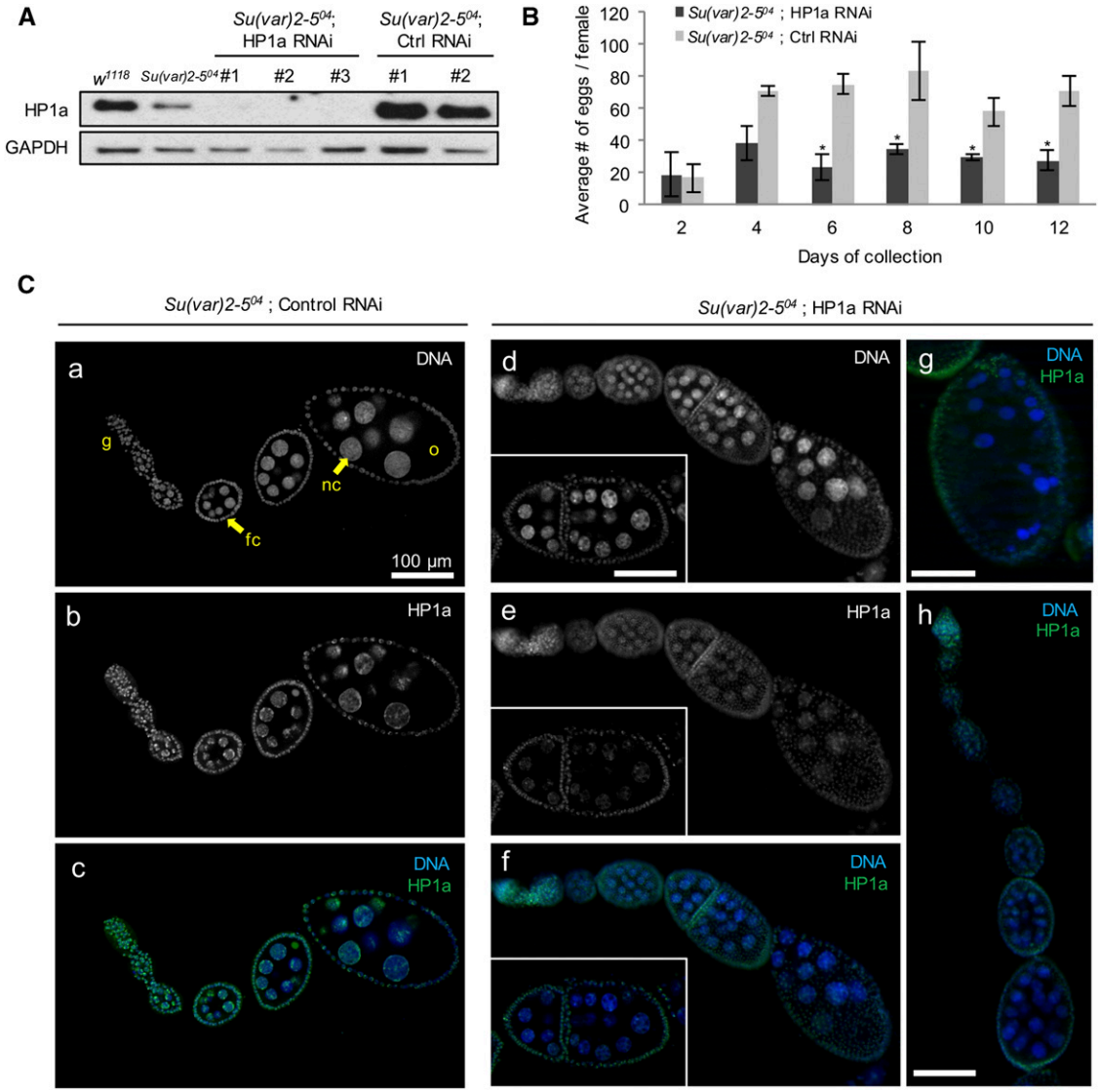


**Figure 1** HP1a reduction during mid- and late-stage oogenesis leads to defects in ovarian morphology and subfertility. (A) HP1a expression is reduced significantly in HP1a RNAi ovaries. Immunoblot of wild-type, *Su(var)2-5$^{04}$* heterozygous, HP1a RNAi, and control EGFP RNAi ovaries. HP1a RNAi #1 is obtained from the Transgenic RNAi Project and HP1a RNAi #2 is newly generated in this study (Supplemental Material). HP1a RNAi #3 is a third HP1a RNAi line that was generated to target a different site on HP1a and was not used in this study. Ctrl RNAi corresponds to EGFP RNAi with the same insertion sites. HP1a level is reduced to one-half the amount of *w$^{1118}$* (wild-type) in *Su(var)2-5$^{04}$* heterozygotes, while HP1a is reduced to an undetectable amount in HP1a RNAi ovaries. HP1a level is slightly higher than that of *w$^{1118}$* control and the EGFP control RNAi flies. GAPDH expression serves as a loading control. (B) Fertility is significantly reduced in HP1a-deficient females. Eggs collected in females from each HP1a RNAi (#1 and #2) and control RNAi (#1 and #2) in the *Su(var)2-5$^{04}$* heterozygous background were counted on days 2, 4, 6, 8, 10, and 12. The average number of eggs laid in the two HP1a RNAi lines and the control RNAi lines was calculated for each day. Starting on day 6, HP1a-deficient females laid significantly fewer eggs than the control females. * *P*-value ≤ 0.05. *n*, HP1a RNAi = 540; *n*, control RNAi flies: 1101. Error bars indicate the mean value ± SEM in three biological replicates. (C) HP1a RNAi ovaries exhibit various morphological and nuclear defects. HP1a expression was detected using anti-HP1a antibody labeling. (a–c) Confocal micrographs of the control EGFP RNAi ovariole in the *Su(var)2-5$^{04}$* heterozygous background. The HP1a expression level shown in (b) is comparable to that of the *w$^{1118}$* or *Su(var)2-5$^{04}$* heterozygous ovarioles (data not shown), and no defects or abnormalities in the ovarian morphology are detected. (d–h) Confocal micrographs of HP1a RNAi ovarioles and egg chambers in the *Su(var)2-5$^{04}$* heterozygous background. (e) shows a diminished level of HP1a expression throughout the HP1a RNAi ovariole. The insets in (d–f) highlight two joined egg chambers with multiple nuclei. (g) An egg chamber with overcondensed nuclei. (h) An ovariole with a series of early stage egg chambers. EGFP, enhanced GFP; fc, follicle cell; g, germarium; nc, nurse cell; o, oocyte; RNAi, RNA interference.

(Supplemental Material). EGFP RNAi lines #1 and #2, which produce shRNA against EGFP sequences from the same insertion site as HP1a RNAi #1 and #2 lines, respectively, were used as position-effect controls.

We first reduced HP1a expression in the entire ovarian germline using a maternal triple-GAL4 driver (Petrella *et al.* 2007). As a result, both ovary formation and oogenesis were severely affected, leading to rudimentary ovary development

**Table 1 HP1a-deficient ovaries exhibit various nuclear defects**

| Genotype | Multiple nuclei | Overcondensed nuclei | Joined egg chambers | Accumulation of early stage egg chambers | *n* |
|---|---|---|---|---|---|
| $w^{1118}$ | 0 | 6 (0.0%) | 0 | 0 | 344 |
| *Su(var)2-5*$^{04}$ | 4 (0.0%) | 6 (0.0%) | 0 | 0 | 484 |
| *Su(var)2-5*$^{04}$; HP1a RNAi#1 | 248 (74.6%) | 194 (58.4%) | 92 (27.7%) | 68 (20.4%) | 332 |
| *Su(var)2-5*$^{04}$; EGFP RNAi#1 | 8 (0.0%) | 10 (0.0%) | 0 | 2 (0.0%) | 396 |
| *Su(var)2-5*$^{04}$; HP1a RNAi#2 | 280 (85.3%) | 172 (52.4%) | 180 (34.1%) | 46 (14.0%) | 528 |
| *Su(var)2-5*$^{04}$; EGFP RNAi#2 | 16 (0.0%) | 4 (0.0%) | 4 (0.0%) | 0 | 412 |

For each genotype, the percentage of ovarioles with the indicated phenotypes was calculated from the total number (*n*) counted in two independent experiments. "Multiple nuclei" indicates > 16 nuclei in an egg chamber (refer to Figure 1C, e and f). The percentage reported in the *Results* section is the average percentage from those of HP1a RNAi #1 and HP1a RNAi #2. RNAi, RNA interference; EGFP, enhanced GFP.

and an absence of egg production, as previously reported (Yan *et al.* 2014). This indicates the important function of HP1a in ovarian development as well as in oogenesis.

We then reduced HP1a expression in mid- to late-stage egg chambers to examine the function of HP1a in the expression of maternal transcripts without overly affecting ovary formation or oogenesis. This was achieved by using a maternal α-tubulin GAL4 driver (Staller *et al.* 2013). Inducing HP1a RNAi #1 in the wild-type background did not result in any observable phenotype in the ovary or the embryos. To achieve a greater reduction of HP1a expression, we induced RNAi in the heterozygous *Su(var)2-5*$^{04}$ background. *Su(var)2-5*$^{04}$ is a nonsense mutation in the chromo shadow domain of HP1a, which leads to the deletion of the domain that is required for HP1a localization to the nucleus (Eissenberg *et al.* 1992). From here on, all HP1a RNAi and EGFP control RNAi refer to those induced in the *Su(var)2-5*$^{04}$ heterozygous background.

We first assessed the knockdown efficiency of both HP1a RNAi lines by immunoblot (Figure 1A) and fluorescence studies (Figure 1C). Both lines showed efficient reduction of HP1a expression, with HP1a undetectable on the immunoblot (Figure 1A). Increased HP1a expression was detected in the EGFP HP1a RNAi lines, but ovarian morphology, egg deposition, and hatching rates in these flies were comparable to those observed in the wild-type flies (Figure 1B), indicating normal fertility and embryo viability. To examine the effect of reducing HP1a expression during oogenesis, we dissected ovaries from HP1a-deficient flies and probed for HP1a expression using an anti-HP1a antibody. HP1a expression was much lower in the HP1a RNAi ovaries (Figure 1C, a–h). Various defects were observed in HP1a-deficient ovaries, including multinucleated and joined egg chambers (Figure 1C, d–f), overcondensed nuclei (Figure 1C, g), and mild accumulation of early-stage egg chambers (Figure 1C). Quantification of the ovarian effects in both HP1a RNAi lines relative to their corresponding EGFP RNAi controls are shown in Table 1. The females with reduced HP1a expression also showed compromised fertility. The average number of eggs laid by these females was significantly lower, compared to those laid by corresponding EGFP control females, which showed similar rates as those of wild-type females (Figure 1B). The ovarian defects and subfertility caused by a reduction in HP1a expression confirm that HP1a is essential for oogenesis. Meanwhile, the subfertility allowed us to examine the effect of reducing HP1a expression during oogenesis on embryogenesis.

### *Embryos with a reduced load of maternal HP1a are developmentally delayed or arrested*

We examined how the reduction of maternal HP1a expression affects the early nuclear divisions of embryos. We first confirmed that embryos from mothers with a reduced HP1a expression inherit a decreased amount of HP1a as compared to control embryos (Figure 2A, a similar level of reduction was observed in HP1a RNAi #1, data not shown). We then determined the embryonic stage that solely relies on maternally loaded HP1a by detecting when the paternal allele of HP1a is first expressed during embryogenesis. To label the paternal allele of HP1a, we created an EGFP-HP1a knock-in fly using CRISPR/Cas9 (Supplemental Material; this is not to be confused with EGFP RNAi control lines, which were used as controls to target EGFP in non-EGFP-HP1a flies). EGFP-HP1a knock-in males were crossed to wild-type females to selectively label the paternal zygotic copy of HP1a in the embryo. The paternal zygotic transcript of HP1a was first detected at cycle 12 (Figure 2B) and the HP1a protein at cycle 14 (Figure 2C). To examine if there was any defect in the embryos laid by HP1a-deficient females, we collected their eggs and scored the average percentage of embryos that hatched (Figure 2D). While wild-type, *Su(var)2-5*$^{04}$ heterozygous mutant, and EGFP RNAi control females showed similar hatch rates, no embryo from HP1a RNAi mothers hatched.

To investigate whether the embryos from HP1a-deficient mothers were arrested due to developmental delay, we collected newly laid eggs for 2 hr and incubated them for 3 hr before examination to obtain 3–5 hr embryos. Embryos from HP1a-deficient mothers [HP1a RNAi in the *Su(var)2-5*$^{04}$ heterozygous background] exhibited developmental arrest and delayed development in various stages (Figure 2, E and F). Among the 3–5-hr-old embryos, 98% of control embryos [EGFP RNAi in the *Su(var)2-5*$^{04}$ heterozygous background] were in postcycle 14 (cycle 14+), as expected from embryos grown at 25°C (Foe *et al.* 1993), while only 5% of embryos from HP1a-deficient mothers reached postcycle 14 (Figure 2E). Many of the embryos were developmentally arrested starting at cycle 1 (24.2%, $n = 48$; Figure 2F and Figure 3A, a) and others showed varying degrees of delayed

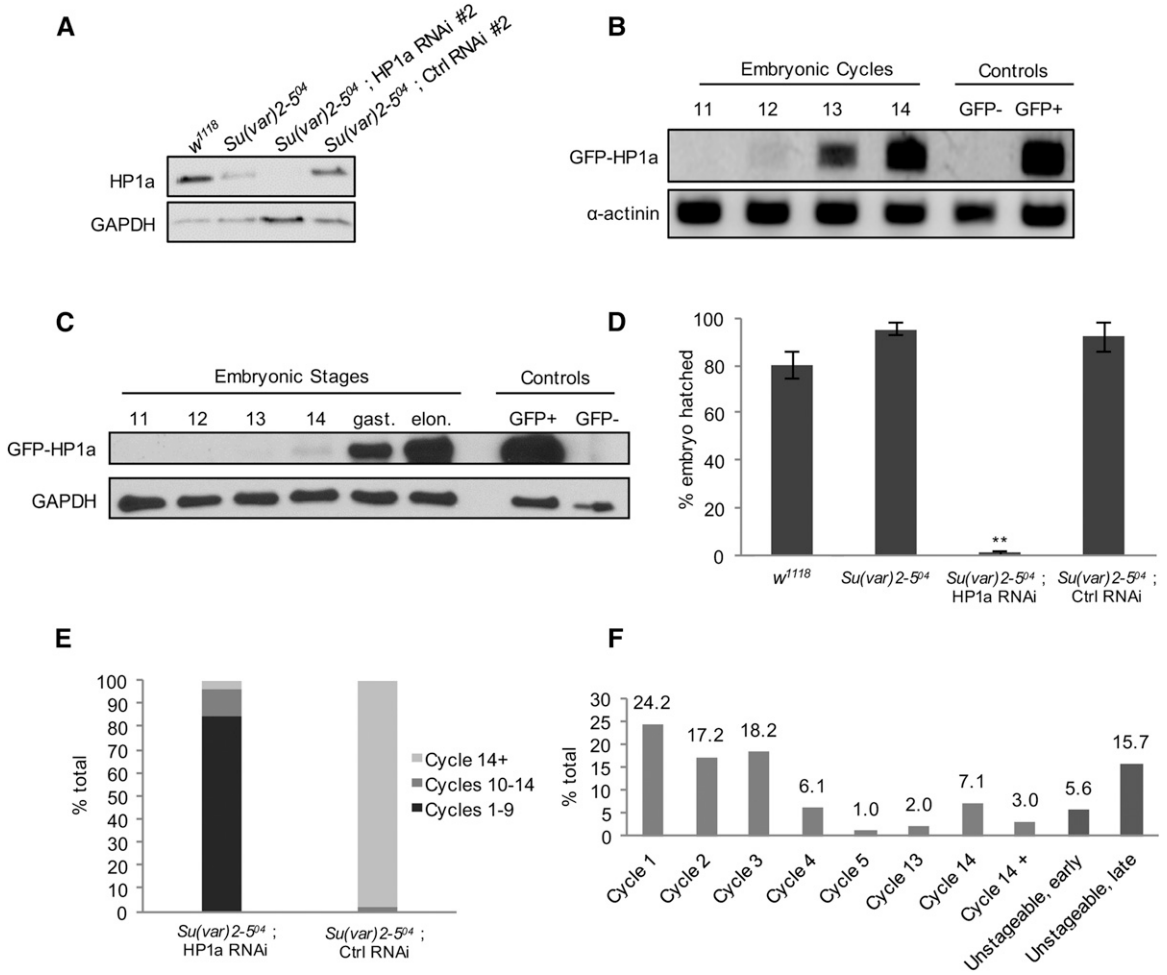


**Figure 2** Embryos with a reduced load of maternal HP1a are developmentally delayed or arrested. (A) Embryos from HP1a-deficient females inherit a reduced amount of HP1a. HP1a expression levels in stage 14 eggs (equivalent to unfertilized embryo) collected from $w^{1118}$, *Su(var)2-5*$^{04}$ heterozygote, *Su(var)2-5*$^{04}$/+ ; HP1a RNAi #2, and *Su(var)2-5*$^{04}$/+ ; control RNAi #2 females. Embryos from an HP1a RNAi female show an undetectable level of HP1a. GAPDH expression serves as a loading control. (B and C) The Zygotic transcript of HP1a is first detected at cycle 12 and protein at cycle 14. Wild-type females were crossed to EGFP-HP1a knock-in males to selectively label the paternal zygotic copy of HP1a. Embryos at different stages were collected, and probed for the presence of newly transcribed and translated paternal zygotic copies of EGFP-HP1a. (B) The GFP-HP1a transcript is first detected in embryonic cycle 12. Embryos collected from $w^{1118}$ females were used as the GFP-negative control and those collected from a transgenic GFP-HP1a line (#30561; Bloomington *Drosophila* Stock Center) were used as the GFP+ control. The α-actinin transcript was probed as a loading control. (C) GFP-HP1a protein is first detected in embryonic cycle 14, and is expressed in an increasing manner in the later gastrulation and elongation stages. Embryos collected from $w^{1118}$ females were used as the GFP-negative control and those collected from a transgenic GFP-HP1a (#30561; Bloomington *Drosophila* Stock Center) were used as the GFP+ control. GAPDH was probed as a loading control. (D) Embryos from females with the following genotypes, $w^{1118}$, *Su(var)2-5*$^{04}$ heterozygous, HP1a RNAi (#1 and #2), and control RNAi (#1 and #2) in the *Su(var)2-5*$^{04}$ heterozygous background, were collected and the number of embryos hatched was scored after 30 hr. The average hatching rate was 80% or above in the $w^{1118}$, *Su(var)2-5*$^{04}$ heterozygous, and control RNAi samples, while embryos from HP1a RNAi females did not hatch. ** *P*-value ≤ 0.001. *n*, $w^{1118}$ = 382; *n*, *Su(var)2-5*$^{04}$ = 429; *n*, HP1a RNAi = 540; and *n*, control RNAi = 1101. Error bars indicate the mean percentage ± SEM in three biological replicates. (E) Embryos from HP1a-deficient females are developmentally delayed or arrested. The 3–5-hr-old embryos were staged and counted. In embryos from HP1a-deficient females, 85% of the embryos are in cycles 1–9, 10% in cycles 10–14, and 5% beyond cycle 14. In embryos from control females, 98% are in cycle 14 or beyond and 2% are in cycles 10–14. These values do not include the unstageable, early-, and late-stage embryos shown in (F). Embryo counts from both HP1a RNAi lines (#1 and #2) and control RNAi lines (#1 and #2) in the *Su(var)2-5*$^{04}$ heterozygous background were averaged in each biological replicate. The overall mean percentage was calculated from two biological replicates. *n*, HP1a RNAi = 342; *n*, control RNAi = 412. (F) Distribution of embryonic stages in embryos from HP1a-deficient females. Each 3–5-hr-old embryo was scored according to mitotic cycles. Of the embryos, 60% are arrested at cycles 1–3, and 10% of the embryos were found at cycle 14 or beyond. Nuclear organization in 21% of the embryos was highly disrupted and was categorized as unstageable, early (before cycle 14), or unstageable, late (cycle 14 or beyond). Embryo counts from both HP1a RNAi lines (#1 and #2) in the *Su(var)2-5*$^{04}$ heterozygous background were averaged in each biological replicate. The overall mean percentage was calculated from two biological replicates. *n* = 342. Ctrl, control; EGFP, enhanced GFP; RNAi, RNA interference.

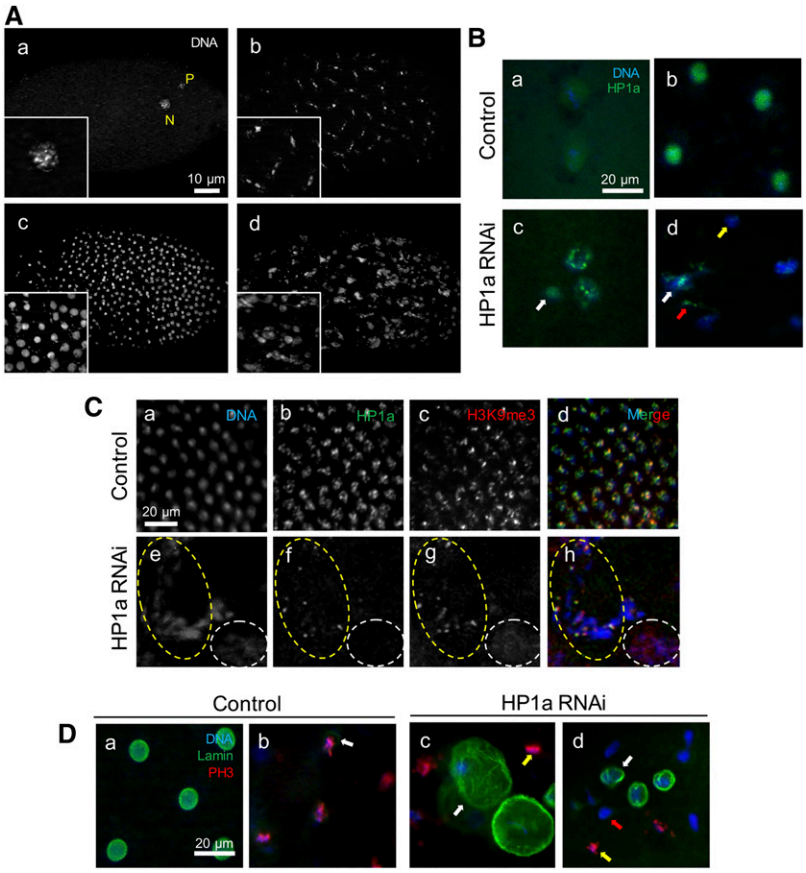


**Figure 3** Nuclear defects and HP1a distribution in embryos from HP1a-deficient mothers. "Control" refers to embryos from females with EGFP RNAi #2 induced in the *Su(var)2-5*$^{04}$ heterozygous background and *HP1a RNAi* embryos are from females with HP1a RNAi #2 induced in the *Su(var)2-5*$^{04}$ heterozygous background. Comparable expressions are observed in the EGFP RNAi #1 and HP1a RNAi #1 lines induced in the *Su(var)2-5*$^{04}$ heterozygous background, and quantifications of the defects along with the *w*$^{1118}$ and *Su(var)2-5*$^{04}$ heterozygous controls are presented in Table 2. (A) Embryos from HP1a-deficient mothers exhibit various nuclear defects. Embryos from HP1a RNAi females in a 3–5-hr collection were fixed and stained with DAPI for characterization of nuclear defects. Each panel shows a whole embryo and insets provide close-up views of the nuclear defects. (a) Embryo with multiple, fragmented nuclei arrested at cycle 1; N, nucleus; *P*, polar body. (b) Asynchronous division in cycle 7 embryo with anaphase and interphase nuclei. (c) Overcondensed nuclei. (d) Heterogeneous defects in nuclear morphology and organization. The scale bar in (a) also applies to (b–d). (B) Embryos from HP1a-deficient females display reduced expression and heterogeneous localization of HP1a compared to those from control females. HP1a expression was detected using anti-HP1a antibody labeling. (a) Maternal HP1a is expressed throughout the embryo and at a slightly high level surrounding the nucleus in cycle 1. (b) HP1a expression correlates to that of the nuclei in the control embryo in cycle 5. (c) HP1a expression is reduced throughout the embryo and expressed in puncta in fragmented nuclei. The white arrow indicates heterogeneous HP1a expression in an aberrant nuclei. (d) Nuclei in embryos from HP1a-deficient mothers are irregular and are loosely associated with HP1a (white arrow). Some HP1a expression is not associated with nuclei (red arrow) while some nuclei are organized in the absence of HP1a expression (yellow arrow). The scale bar in (a) also applies to (c–d). All expression was detected using antibody labeling. (C) Costain of HP1a and H3K9me3 expression. (a–d) HP1a and H3K9me3 expression is nuclear, and regions of concentrated expression are correlated in the control embryo. (e–f) HP1a and H3K9me3 expression in embryos from HP1a-deficient females. The yellow dotted circle indicates a region where HP1a and H3K9me3 are coexpressed over a condensed chromatin structure. The white dotted circle indicates a region where both HP1a and H3K9me3 expression are missing with diffused chromatin structure. The scale bar in (a) also applies to (b–h), and all expression was detected using antibody labeling. (D) Nuclear lamin and PH3 expression in the (a and b) control and (c and d) HP1a-deficient embryos. (a) Lamin demarcates a clear nuclear boundary during interphase and no PH3 expression is detected. (b) Nuclear lamin is faint (white arrow) or nonexistent in metaphase nuclei, which express PH3. (c) Enlarged nuclear boundary (white arrow) and an adjacent nucleus in mitosis (yellow arrow) is observed within the same HP1a-deficient embryo. (d) Irregular lamin expression (white arrow), absence of lamin expression in a mitotic nucleus (yellow arrow), and absence of lamin expression in a nonmitotic nucleus (red arrow) are observed within the same HP1-deficient embryo. The scale bar in (a) also applies to (b–d). All expression was detected using antibody labeling. EGFP, enhanced GFP; RNAi, RNA interference.

development in various stages (Figure 2F). Many embryos were developmentally arrested at cycles 1–3, while the ones that escaped developed beyond those cycles. Embryos from HP1a-deficient mothers also exhibited gross nuclear defects, and many were classified as early (likely containing cycles 6–12) or late (cycle 14 or later) embryos with the exact cell cycle unstageable (Figure 2F; denoted as "unstageable, early" and "unstageable, late," respectively).

### *Maternal HP1a-deficient embryos exhibit various nuclear defects*

We then characterized nuclear defects that were observed in these developmentally delayed embryos. Figure 3A, a shows a developmentally arrested embryo at cycle 1. In pregastrulation embryos, various defects, including multinucleation (Figure 3A, a), asynchronous nuclear division (Figure 3A, b), and overcondensed nuclei (Figure 3A, c) are observed. Multiple categories of the above defects were often observed within a single embryo (Figure 3A, d). Table 2 shows quantification of these embryonic effects in both HP1a RNAi lines relative to their corresponding EGFP RNAi controls [all in the *Su(var)2-5*$^{04}$ heterozygous background]. Overall, the percentage of embryos with each defect was higher in embryos from HP1a RNAi #2 mothers than those from HP1a RNAi #1 females. Despite this, a similar trend was observed in both HP1a RNAi lines. On average, 75.6% of all HP1a-deficient embryos exhibited asynchronous nuclear division, while $>$ 50% of all HP1a-deficient embryos contained overcondensed and multiple nuclei (Table 2).

As expected, HP1a expression was reduced in embryos from HP1a-deficient mothers. In an early-stage control embryo from mothers with EGFP control RNAi in the *Su(var)2-5*$^{04}$ heterozygous background, maternal HP1a was expressed throughout the embryo, with an accentuated level surrounding

**Table 2 Quantification of nuclear abnormalities in embryos from HP1a-deficient mothers**

| Maternal genotype | Multiple nuclei | Overcondensed nuclei | Asynchronous nuclear division | *n* |
|---|---|---|---|---|
| $w^{1118}$ | 8 (0.0%) | 4 (0.0%) | 14 (0.1%) | 268 |
| *Su(var)2-5*$^{04}$ | 8 (0.0%) | 6 (0.0%) | 6 (0.0%) | 324 |
| *Su(var)2-5*$^{04}$; HP1a RNAi#1 | 286 (40.6%) | 386 (54.8%) | 484 (68.8%) | 704 |
| *Su(var)2-5*$^{04}$; EGFP RNAi#1 | 4 (0.0%) | 2 (0.0%) | 12 (0.0%) | 400 |
| *Su(var)2-5*$^{04}$; HP1a RNAi#2 | 354 (64.8%) | 180 (65.9%) | 450 (82.4%) | 546 |
| *Su(var)2-5*$^{04}$; EGFP RNAi#2 | 6 (0.0%) | 2 (0.0%) | 16 (0.0%) | 506 |

For each maternal genotype, the percentage of embryos with the indicated phenotypes was calculated from the total number (*n*) counted in two independent experiments. "Multiple nuclei" indicates fragmented nuclei. The total number counted (*n*) for HP1a and H3K9me3 was the same (counted from costained preparations) and are presented in a common column between the two. The percentage reported in the *Results* section is the average percentage from those of HP1a RNAi #1 and HP1a RNAi #2. RNAi, RNA interference; EGFP, enhanced GFP.

the nucleus (Figure 3B, a). However, in an embryo from an HP1a-deficient mother [HP1a RNAi in the *Su(var)2-5*$^{04}$ heterozygous background], HP1a expression was overall low and not uniform in all nuclei. In Figure 3B, c, HP1a is expressed in puncta within nuclei, which indicates more condensed chromatin. An even HP1a expression that lacked distinct puncta was observed in the smaller, aberrant nuclei nearby (Figure 3B, c; white arrow), which indicates that HP1a expression reflects heterogeneity in nuclear organization (Figure 3B, c; arrow). As the cell cycle progressed, HP1a expression directly correlated with that of the nuclei in the control embryo (Figure 3B, b). While in embryos with a reduced load of maternal HP1a, nuclei were loosely associated with HP1a (Figure 3B, d; white arrow) and scattered HP1a expression was observed even where nuclei were absent (Figure 3B, d, red arrow). In some nuclei, HP1a expression was missing altogether, even though nuclear organization was maintained (Figure 3B, d; yellow arrow). Quantification of these heterozygous HP1a expression patterns is presented in Table 3.

We also examined whether H3K9me3 expression was disrupted in HP1a-deficient embryos by costaining HP1a, H3K9me3, and DNA within the same embryos. In the control embryos, HP1a expression was nuclear, where it was in distinct puncta over more condensed chromatin (Figure 3C, b). H3K9me3 expression correlates to that of HP1a (Figure 3C, c and d). However, in embryos from an HP1a-deficient mother, HP1a was often expressed in concentrated spots along a stretch of DNA (Figure 3C, e–h; yellow dotted circle) but absent in a more diffused nuclear area (Figure 3C, e–h; white dotted circle).

H3K9me3 expression was also always directly correlated with HP1a expression and the overall nuclear organization in the HP1a-deficient embryos, as H3K9me3 was also expressed in concentrated spots but was unorganized where HP1a expression is absent (Figure 3C, e–h and Table 3). In both control and HP1a-deficient embryos, H3K9me3 expression was directly correlated with that of HP1a, indicating that HP1a binds to H3K9me3 in both wild-type and HP1a-deficient embryos.

The disrupted nuclear organization in HP1a-deficient embryos was also indicated by lamin staining. In the control embryos at interphase, each nucleus was marked and surrounded by a distinct nuclear boundary (Figure 3D, a). In embryos from HP1a-deficient mothers, nuclear lamin was enlarged to house multiple scattered nuclei (Figure 3D, c; white arrows), which were sometimes irregularly shaped (Figure 3D, d; white arrow) or even absent. To investigate whether this is due to defects in nuclear division, potentially leading to the accumulation of nuclei that are arrested or delayed in completing mitosis, we costained the same embryos with lamin and PH3, a mitosis marker. In the control embryos, nuclear lamin was not present or faintly expressed in all nuclei that were in metaphase (Figure 3D, b; arrow). Furthermore, a distinct nuclear boundary was observed in all nuclei during interphase (Figure 3D, a). However, in embryos from HP1a-deficient mothers, we detected mitotic nuclei without lamin (Figure 3D, c and d; yellow arrows). Moreover, lamin was absent even in some interphase nuclei (Figure 3D, d; red arrow; Table 3). The lack of localization of lamin at the nuclear periphery did not always correlate to nuclear division or defects thereof. This indicates that HP1a deficiency not only leads to developmental delay or arrest, but also plays an important function in nuclear organization in early embryos.

### *Maternal HP1a-deficient embryos exhibit various mitotic defects*

We further examined the effect of maternal HP1a deficiency on nuclear divisions during early embryogenesis by staining these embryos with mitotic markers. In the control embryos, microtubules were clearly visible as mitotic spindles that sandwich dividing chromosomes of all nuclei (Figure 4A, a). However, in embryos from HP1a-deficient mothers, some nuclei were no longer associated with tubulin (Figure 4A, b; white arrow) and microtubule organization was severely aberrant, as shown by diffuse mitotic spindles (Figure 4A, c; white arrow). Furthermore, different nuclei in the same embryos were in various stages of mitosis, clearly indicating asynchronous mitosis (Figure 4A, c; both arrows).

We also examined centrosomin, a marker for centrosomes and mitotic spindle organization. Nuclei in the control embryo were surrounded by a pair of distinct centrosomin dots (Figure 4B, a), indicating the presence of two centrosomes. However, in embryos from HP1a-deficient mothers, some nuclei lacked centrosomes (Figure 4B, b; yellow arrow), while free-floating

**Table 3 Disrupted nuclear organization in embryos from HP1a-deficient mothers**

| Maternal genotype | HP1a | | | *n* | H3K9me3 Not correlated with HP1a expression | Lamin | | | | *n* |
|---|---|---|---|---|---|---|---|---|---|---|
| | Scattered puncta | Diffuse, not associated with nuclei | Absent | | | Irregular | Enlarged | Absent (+PH3) | Absent (−PH3) | |
| $w^{1118}$ | 3 (0.0%) | 2 (0.0%) | 0 | 382 | 0 | 6 (0.0%) | 0 | 12 (0.0%) | 3 (0.0%) | 500 |
| *Su(var)2-5*$^{04}$ | 10 (0.0%) | 0 | 0 | 465 | 0 | 4 (0.0%) | 1 (0.0%) | 8 (0.0%) | 0 | 456 |
| *Su(var)2-5*$^{04}$; HP1a RNAi#1 | 500 (77.8%) | 482 (75.1%) | 472 (73.5%) | 642 | 0 | 552 (80.2%) | 186 (27.0%) | 214 (31.1%) | 15 (0.0%) | 688 |
| *Su(var)2-5*$^{04}$; EGFP RNAi#1 | 4 (0.0%) | 2 (0.0%) | 0 | 500 | 0 | 5 (0.0%) | 0 | 15 (0.0%) | 218 (47.8%) | 556 |
| *Su(var)2-5*$^{04}$; HP1a RNAi#2 | 352 (76.9%) | 360 (78.6%) | 360 (78.6%) | 458 | 0 | 431 (76.4%) | 141 (25.0%) | 225 (39.9%) | 20 (0.0%) | 564 |
| *Su(var)2-5*$^{04}$; EGFP RNAi#2 | 16 (0.0%) | 1 (0.0%) | 0 | 520 | 0 | 5 (0.0%) | 0 | 16 (0.0%) | 200 (44.9%) | 445 |

For each maternal genotype, the percentage of embryos with the indicated phenotypes was calculated from the total number (*n*) counted in two independent experiments. "Absent" under HP1a expression indicates no HP1a expression on a nucleus. The total number counted (*n*) for HP1a and H3K9me3 was the same (counted from costained preparations) and are presented in a common column between the two. Percentage reported in the *Results* section is the average percentage from those of HP1a RNAi #1 and HP1a RNAi #2. "Lamin, Absent (+PH3)" denotes absence of lamin expression in a mitotic (PH3-expressing) cell. "Lamin, Absent (-PH3)" denotes absence of lamin expression in a non-mitotic (not expressing PH3) cell. RNAi, RNA interference; EGFP, enhanced GFP.

doublets of centrosomes that did not seem to be associated with any nuclei were also observed in 83.6% of the HP1a-deficient embryos (Figure 4B, c; white arrow, Table 4). Nuclei that were loosely organized were surrounded by multiple centrosomin spots (Figure 4B, b; white arrow).

To further characterize the asynchronous division in the HP1a-deficient embryos, we examined PH3 localization more closely. In the control embryos, PH3 was localized uniformly in all nuclei going through synchronous nuclear division (Figure 4C, a). However, in HP1a-deficient embryos, PH3 localization was not uniform, as we found nuclei without PH3 (Figure 4C, c; white arrow) and abnormally high PH3 localization that reflects disrupted nuclear organization (Figure 4C, c; yellow arrow) within the same embryo. Together, microtubule, centrosomin, and PH3 staining revealed severe defects in the mitotic apparatus, as well as asynchrony of mitosis in embryos from HP1a-deficient females. Quantification of these defects is presented in Table 4.

To investigate whether the mitotic defects observed in HP1a-deficient embryos are spatially correlated with HP1a localization, we costained HP1a and tubulin within the same embryos. In the control embryos, HP1a dissociates from the nuclei in metaphase (Figure 4D, b). Microtubules formed mitotic spindles associated with dividing chromosomes (Figure 4D, c). However, in 70.1% of HP1a-deficient embryos, we detected tubulin organization as mitotic spindles around disorganized chromatins where HP1a expression was absent (Figure 4D, g; yellow arrow; and Table 4). Conversely, in 40.2% of the HP1a-decifient embryos, we also observed that tubulin organization was absent in nuclei with normal HP1a localization (Table 4). These observations indicate that mitotic defects may not be always directly caused by defects or an absence of HP1a. Instead, maternal genes and pathways that were disrupted by reduced maternal HP1a expression may also contribute to the gross misorganization of the nuclear structure.

### *HP1a deficiency during oogenesis disrupts the expression of maternal transcripts that regulate translation, mitosis, and later-stage developmental processes*

Maternal transcripts are made in the nurse cells and passed onto the oocyte around oogenic stage 10 via a process called nurse cell dumping (Gutzeit and Koppa 1982). To identify maternal transcripts that are regulated by HP1a, we isolated mRNA from stage 14 eggs of HP1a knockdown and EGFP knockdown control females. These stage 14 eggs have completed oogenesis but have not yet been fertilized, thus allowing us to collect a pure population of maternal transcripts right before embryogenesis. By using stage 14 eggs, we could avoid the issue of collecting early embryos that are inevitably at different mitotic cycles, and thus have different compositions of maternal and potentially zygotic transcripts. The mRNA isolated from these stage 14 eggs was then deep-sequenced to identify genes that were differentially expressed upon knocking down HP1a. We also collected mRNA from whole ovaries and compared the maternal transcriptome to the ovarian transcriptome (Supplemental Material). Three biological replicates of stage 14 egg mRNA sequencing were used. Results from these replicates were highly correlated (Figure S1; for bioinformatic pipeline, see Figure S2A).

To obtain a final list of maternal transcripts that were differentially expressed upon reducing HP1a expression, we eliminated genes that were differentially expressed in the corresponding EGFP control RNAi samples to rule out the position-effect variation caused by the different insertion sites of HP1a shRNA. Instead, we only considered mRNAs that were present and showed a consistent trend of changes in both HP1a RNAi lines to rule out the RNAi off-target effect (Figure 5A). We identified 2001 and 4957 mRNAs that were differentially expressed in maternal transcripts from HP1a RNAi #1 and #2 females, respectively, with *P*-values $\leq$ 0.05. Among them, 1450 mRNAs were identified in both HP1a

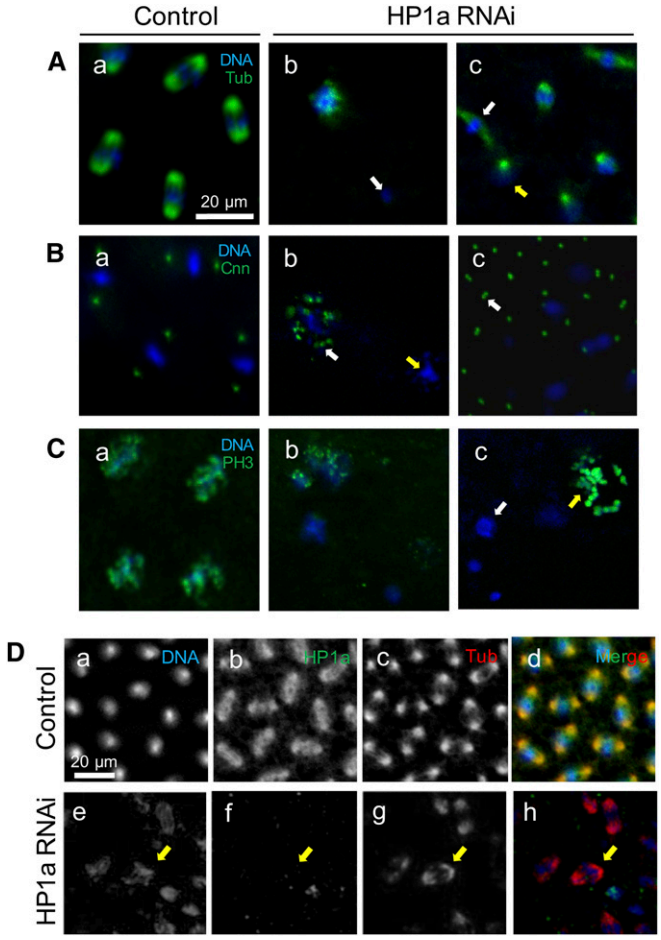


**Figure 4** Maternal HP1a-deficient embryos exhibit various mitotic defects. (A–C) All (a) panels: control embryos from females with EGFP RNAi #2 in the *Su(var)2-5*$^{04}$ heterozygous background; all expression patterns were comparable to embryos from females with EGFP RNAi #1 in the *Su(var)2-5*$^{04}$ heterozygous background, and *w*$^{1118}$ and *Su(var)2-5*$^{04}$ heterozygotes mutation. A quantification of defects from all the aforementioned maternal phenotypes is presented in Table 3. All (b) panels: Maternal HP1a-deficient embryos from females with HP1a RNAi #2 in the *Su(var)2-5*$^{04}$ heterozygous background; all expression patterns were comparable to embryos from females with EGFP RNAi #1 in the *Su(var)2-5*$^{04}$ heterozygous background. Scale bar in (A, a) applies to (A–C). All expression was detected using antibody labeling. (A) Tubulin expression. (a) Microtubule expression is detected at the opposite poles surrounding each nucleus in the control embryo. In the HP1a-deficient embryos, nuclei with (b) no tubulin expression (white arrow), and (c) nuclei in metaphase (white arrow) and prophase (yellow arrow), are observed within the same embryo. (B) Cnn expression. (a) Two centrosomin spots surround each nucleus in the control embryo. In the HP1a-deficient embryos, (b) multiple Cnn spots are associated with a loosely organized nucleus (white arrow), while no Cnn is observed (yellow arrow) in a different nucleus in the same HP1a-deficient embryo. (c) A doublet of Cnn (white arrow) is also observed in the HP1a RNAi embryos. (C) PH3 expression. (a) PH3 expression is detected in all nuclei going through mitosis in the control embryo. (b and c) PH3 expression is not uniform within the same HP1a-deficient embryo. (c) Some nuclei lack PH3 expression (white arrow), while some show an overexpression of PH3 that reflects misorganized nuclear structure (yellow arrow). (D) HP1a and tubulin expression in (a–d) control and (e–f) HP1a-deficient embryos. (b) HP1a is dissociated from and loosely surrounds the nuclei going through mitosis, and (c) the mitotic spindle is expressed in the opposite poles around each nucleus during mitosis. (e–h) Yellow arrow indicates a nucleus that (f) lacks HP1a expression but has (g) normal tubulin expression. Scale bar in (a) also applies to (b–h). Cnn, centrosomin; EGFP, enhanced GFP; PH3, phospho histone 3; RNAi, RNA interference; Tub, tubulin.

RNAi lines. Of these 1450 mRNAs, 1359 showed consistent trends in differential expression (Figure 5B), of which 623 (45.8%) were up- and 736 (54.2%) mRNAs were downregulated in both HP1a RNAi lines (Figure 5C).

To examine the function of the HP1a-regulated maternal transcripts, we performed gene ontology analysis for the 623 upregulated and 736 downregulated genes. Top biological functional terms with $P$-value $\leq 0.05$ are plotted in Figure 5, D and E for up- and downregulated genes, respectively. Upregulated genes were involved in physiological regulation, organ growth, and cell fate determination (Figure 5D). These genes include *Sxl*, *sqd*, *nos*, *osk*, *Dip3*, *tkv*, *piwi*, *myo*, and *qin*, whose upregulation was confirmed using qRT-PCR (Figure 5F). In contrast, genes highly enriched in cytoplasmic translation, mitosis, neurogenesis, and mRNA splicing were downregulated in embryos from HP1a-deficient mothers (Figure 5E). Notably downregulated genes include *INCENP*, *AurB*, *CycB3*, *cid*, *Su(var)3-7*, *AGO3*, *Tudor-SN*, *Tdrd3*, and *Orc1*. Downregulation of these genes in embryos from HP1a-deficient mothers was also confirmed using qRT-PCR (Figure 5F).

### *Of the HP1a-regulated genes, 588 are likely direct targets of HP1a*

To identify genes that are directly associated with HP1a during maternal transcript production in the ovary on a genome-wide level, we conducted ovarian HP1a ChIP-seq in biological triplicates (Figure S1). The bioinformatics pipeline and sonication conditions are described in Figure S2B and Figure S3, respectively. Among all identified HP1a-binding regions, 2091 were shared by all three replicates, 809 by two replicates, and 1333 in one replicate (641 in replicate 1, 127 in replicate 2, and 565 in replicate 3; Figure 6A). For downstream analyses, we defined the 2900 regions that were identified in at least two replicates to be HP1a-binding sites. At the genome-wide level, HP1a-binding sites were distributed throughout all chromosomes, in both euchromatic and heterochromatic regions (Figure 6B). Preferential binding was detected in heterochromatic regions, such as the proximal part of chromosome arm 3L, and across the entire chromosomes X and 4 (Figure 6B). Out of all HP1a-binding sites, 78.4% were in coding regions, 19.9% within transposable element repeats, 1.3% in noncoding genes, and 0.4% in intergenic regions (Figure 6C). Furthermore, out of 13,895 protein-coding genes identified in *Drosophila*, 24.5% were identified to be directly associated with HP1a in the ovary (Figure 6D). To examine whether there was any binding pattern in HP1a-bound genes, we conducted metagene analysis and found that HP1a was enriched in the

**Table 4 HP1a-deficient embryos exhibit various mitotic defects**

| Maternal genotype | Tubulin | | | | | Cnn | | | | PH3 | |
|---|---|---|---|---|---|---|---|---|---|---|---|
| | Diffuse spindles | Multiple spindle types (asynch. div.) | Normal expression without HP1a | Absent in the present of HP1a | *n* | Absent | Double | Multiple | *n* | Varied expression (asynch. div.) | *n* |
| *w*$^{1118}$ | 20 (0.0%) | 5 (0.0%) | 0 | 4 (0.0%) | 707 | 0 | 6 (0.0%) | 0 | 488 | 15 (0.0%) | 369 |
| *Su(var)2-5*$^{04}$ | 16 (0.0%) | 2 (0.0%) | 0 | 3 (0.0%) | 554 | 1 (0.0%) | 0 | 2 (0.0%) | 476 | 6 (0.0%) | 552 |
| *Su(var)2-5*$^{04}$; HP1a RNAi#1 | 400 (61.0%) | 460 (70.1%) | 320 (48.8%) | 402 (61.2%) | 656 | 460 (76.8%) | 481 (80.1%) | 403 (67.2%) | 599 | 432 (68.7%) | 629 |
| *Su(var)2-5*$^{04}$; EGFP RNAi#1 | 14 (0.0%) | 0 | 0 | 2 (0.0%) | 465 | 1 (0.0%) | 7 (0.0%) | 0 | 552 | 7 (0.0%) | 443 |
| *Su(var)2-5*$^{04}$; HP1a RNAi#2 | 445 (74.4%) | 485 (81.1%) | 189 (31.6) | 423 (70.7%) | 598 | 503 (78.3%) | 559 (87.0%) | 398 (62.0%) | 642 | 511 (78.6%) | 650 |
| *Su(var)2-5*$^{04}$; EGFP RNAi#2 | 16 (0.0%) | 3 (0.0%) | 0 | 0 | 556 | 0 | 8 (0.0%) | 7 (0.0%) | 494 | 14 (0.0%) | 552 |

For each maternal genotype, the percentage of embryos with the indicated phenotypes was calculated from the total number (n) counted in two independent experiments. "Asynch. div." is short for "asynchronous division." "Multiple spindle types" for tubulin indicates spindles found in multiple stages of mitosis within the same embryo. "Absent" phenotype in Cnn indicates any nucleus with no surrounding Cnn expression. "Varied expression" for PH3 indicates that not all nuclei exhibited uniform PH3 expression (all or none) and thus signifies asynchronous nuclear division. Percentage reported in the *Results* is the average percentage from those of HP1a RNAi #1 and HP1a RNAi #2. asynch. div., asynchronous division; RNAi, RNA interference; EGFP, enhanced GFP.

promoter region 0.5 kb upstream of the TSS (Figure 6E) and in the 3′ UTR region of the associated genes (Figure 6F).

Out of 623 genes that were upregulated upon reducing HP1a expression, 260 genes (41.7%) were directly associated with HP1a, and out of 736 genes that were downregulated upon reducing HP1a level, 328 genes (44.6%) were bound by HP1a. In total, 588 genes out of 1359 differentially expressed genes (43.3%) were bound by HP1a (Figure 5C, $P$-value $< 0.00001$). Using ovary HP1a ChIP-qPCR analysis, we confirmed direct association between differentially regulated maternal transcripts and HP1a (Figure 6G). Among the differentially expressed genes whose levels were confirmed using qRT-PCR (Figure 5F), *piwi*, *myo*, *Tudor-SN*, *AGO3*, *Aurora B*, and *INCENP* are directly associated with HP1a, while *qin*, *oskar*, *Orc1*, and *CycB3* were not directly associated with HP1a (Figure 6G).

We compared the differentially expressed genes and HP1a target genes with the HP1a target genes reported by two previous studies. We first compared our data to HP1a target genes identified in larvae by a ChIP-microarray study by Cryderman *et al.* (2005). Among their HP1a targeted genes, we found that 337 genes have valid FlyBase identifiers (IDs). Among these 337 genes, 61 of them were also identified by our HP1a ChIP-seq as HP1a targets, but only 23 out of 337 were detected by our differential expression analysis. We then compared our data with the HP1a target genes in S2 cells reported by Piacentini *et al.* (2009). It is worth noting that the Piacentini–Fantini study had a different purpose: they used HP1a-RNA immunoprecipitation combined with microarray analysis to pull down HP1a-bound RNA (but not DNA) to investigate HP1a binding to mRNA and RNA pol II. We found that 635 genes from their study have valid FlyBase IDs. Among these 635 genes, 132 of them were also identified by our HP1a ChIP-seq analysis, but 57 out of 635 were detected by our differential expression analysis. These differences are likely due to different tissues as well as different techniques used in these studies.

To examine the global change in the genetic landscape upon reducing HP1a expression, we compared histone modification changes in control and HP1a knockdown ovaries. We saw a decrease in H3K9me3, H3K27me3, and H4Ac expression, yet an increase in H3K4me3 and H2Av marks (Figure S4).

## Discussion

HP1a is a highly conserved chromatin-associated protein that performs numerous functions, including heterochromatin formation, the DNA damage response, regulation of telomere length, mitosis, and transcriptional regulation, which can both activate and silence gene expression (Vermaak and Malik 2009). In this study, we investigated the role of HP1a in the context of development, particularly its global effect on maternal transcriptome production. We identified genes and pathways that are regulated by maternal HP1a in the ovary, and characterized the impact of HP1a regulation on early embryogenesis. These results reveal an essential function of HP1a in ovarian development, oogenesis, and early embryonic development as a maternal regulator.

HP1a has been shown to be involved in mitosis via interaction with other proteins, such as Aurora B. Dissociation of HP1a from heterochromatin by Aurora B via H3S10 phosphorylation is essential during mitosis (Fischle *et al.* 2005; Hirota *et al.* 2005) and for maintaining genome integrity during mitosis (Warecki and Sullivan 2018). HP1a also recruits centromeric proteins, such as INCENP, which is a component of the chromosomal passenger complex along with Aurora B (Ainsztein *et al.* 1998; Ruppert *et al.* 2018). This corrects errors in the attachment of chromosomes to the spindle. In mammalian cells, phosphorylation of HP1α is essential for chromosomal alignment and mitotic progression (Chakraborty *et al.* 2014). Furthermore, Kellum and Alberts showed that HP1a is essential for correct chromosomal segregation in the early *Drosophila* embryo and attributed the

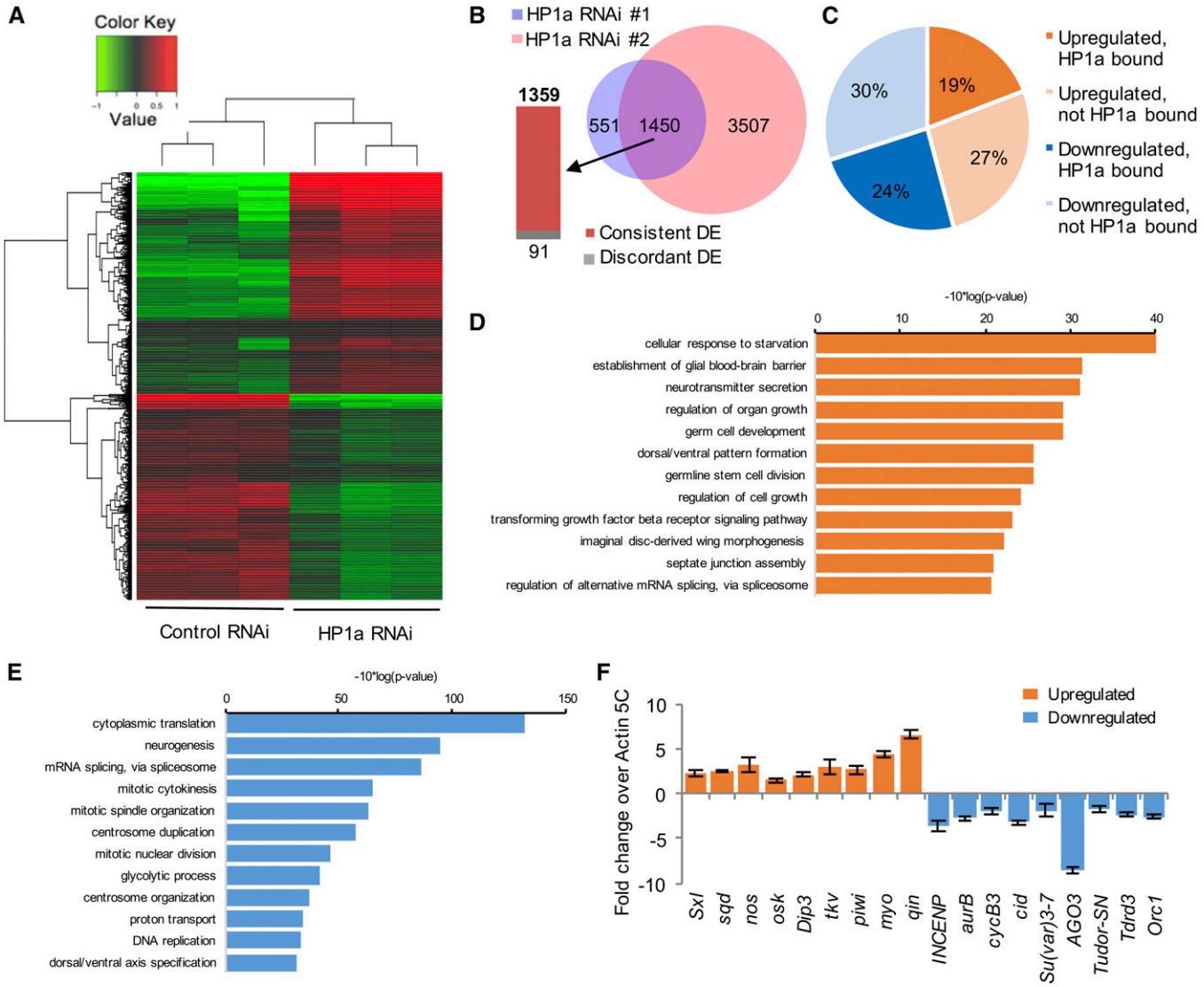


**Figure 5** Bioinformatic analyses of genes differentially expressed upon reducing HP1a expression. (A) A heatmap representing clusters of differentially expressed genes in control and HP1a RNAi lines. (B) In both HP1a RNAi lines, 1450 genes are differentially expressed, among which 1359 genes are consistently DE and 91 genes display an opposite change trend (discordant DE). Of these, 551 genes are differentially expressed and specific to RNAi #1, while 3507 are differentially expressed and specific to RNAi #2. (C) Out of 1359 DE genes that show consistent trends in both HP1a RNAi lines, 19% were upregulated and bound by HP1a, 27% were upregulated but not bound by HP1a, 24% were downregulated and bound by HP1a, and 30% were downregulated but not bound by HP1a, *i.e.*, 43.3% of DE genes were bound by HP1a. (D and E) GO analyses of maternal transcripts differentially expressed upon reducing HP1a expression. (D) GO analysis for upregulated maternal transcripts. Top 12 terms in biological functions with *P*-value ≤ 0.05 are plotted. (E) GO analysis for downregulated maternal transcripts. Top 12 terms in biological functions with *P*-value ≤ 0.05 are plotted. (F) qRT-PCR confirmation of differentially expressed maternal transcripts. Expression levels of genes that are upregulated (orange bars) or downregulated (blue bars) upon HP1a reduction were confirmed in a qRT-PCR experiment. Expression levels are shown as fold change over Cq values for Actin 5C, which did not show a significant level of differential expression upon HP1a reduction. Error bars indicate the mean Cq value ± SEM in three biological replicates. DE, differentially expressed; GO, gene ontology; qRT-PCR; quantitative RT-PCR; RNAi, RNA interference.

cause to a direct role of HP1a in regulating mitosis (Kellum and Alberts 1995). In our study, zygotic HP1a was shown to be transcribed at cycle 12 and translated at cycle 14 (Figure 2, E and F), which indicates that maternal HP1a is responsible for driving embryogenesis up to the maternal-to-zygotic transition that takes place during cycles 12–14. The chromosomal defect in HP1a-deficient embryos may be attributed to the direct participation of HP1a, as supported by the direct correlation between HP1a and H3K9me3 localization. Recent studies by Larson *et al.* (2017) and Strom *et al.* (2017) proposed that heterochromatin formation involves phase separation of HP1a-bound chromatin into liquid-like foci. In embryos with reduced levels of maternal HP1a, we observed spherical HP1a foci that are not associated with chromatin (Figure 3B, f and Figure 4D, e and f), which likely represent free HP1a that forms droplets independent of chromatin due to gross misorganization of the nuclear structure (Strom *et al.* 2017). In the maternal HP1a-deficient embryos, more

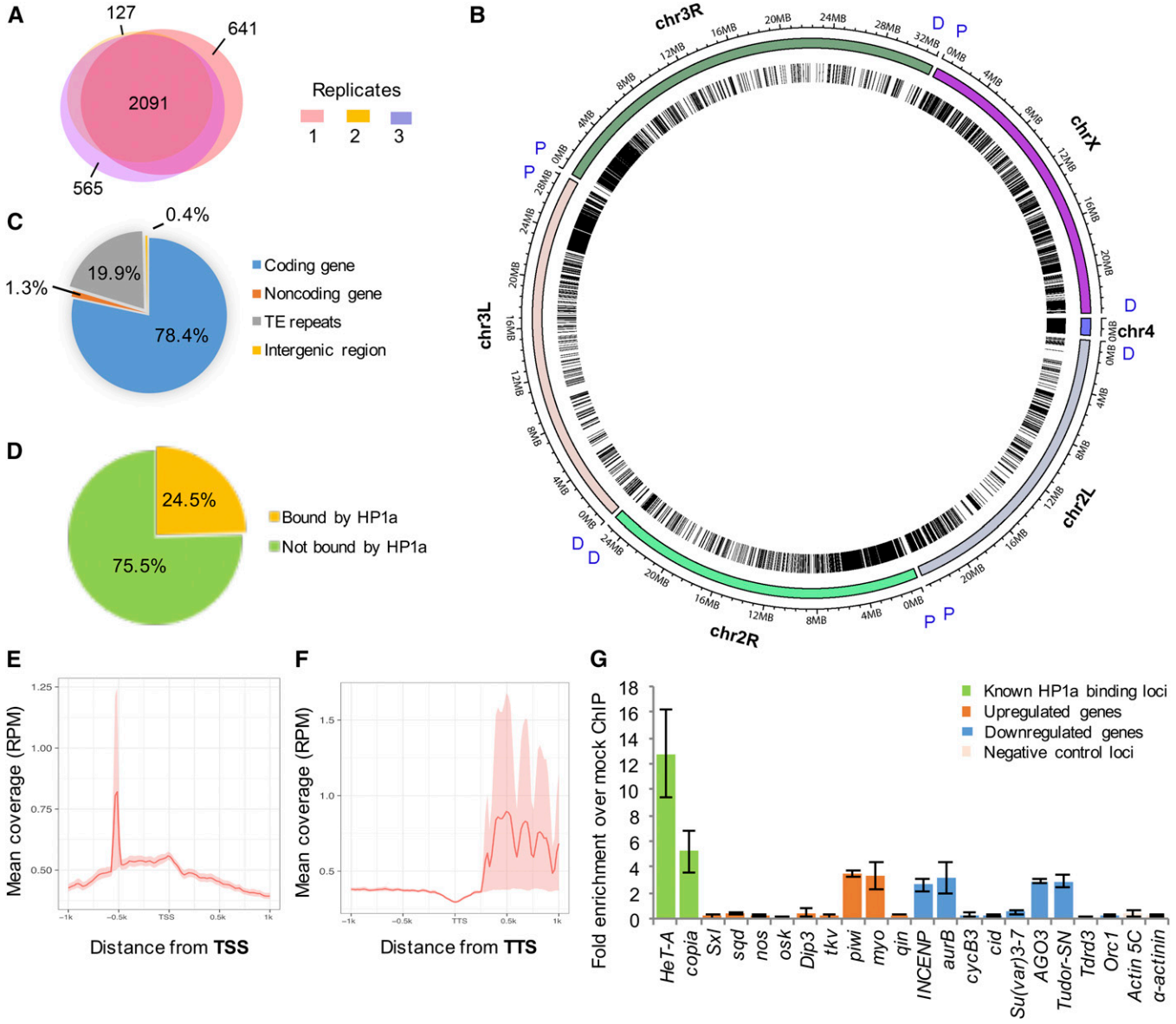


**Figure 6** Summary of HP1a ChIP-seq analysis. (A) HP1a-binding sites were identified in all three biological replicates of HP1a ChIP-seq. In ChIP-seq replicate 1, 3585 regions were identified as HP1a-binding sites, 2914 regions in replicate 2, and 3600 regions in replicate 3. Among all identified HP1a-binding regions, 2091 were shared by all three replicates, 809 by two replicates, and 1333 were captured in only one replicate (641 in replicate 1, 127 in replicate 2, and 565 in replicate 3). In total, 2900 peaks that were identified in at least two biological replicates were considered to be HP1a-binding sites and used for further analyses. (B) Chromosome-based Circos plot of HP1a-binding sites. Chromosome regions 2L, 2R, 3L, 3R, 4, and X are shown and binned at 1-Mb intervals. Proximal (P) and distal (D) parts of each chromosome label are labeled in blue. HP1a-binding sites are represented by single lines within the circle and are distributed throughout all chromosomes, in both euchromatic and heterochromatic regions. Higher HP1a enrichment is detected in heterochromatic regions, such as the proximal part of chromosome arm 3L, and across the entire chromosomes 4 and X. (C) Annotation of HP1a-binding sites. Of these, 78.4% are found in the coding region, 19.9% within transposable element repeats, 1.3% in noncoding RNA genes, and 0.4% in the intergenic region. (D) Out of 13,895 protein-coding genes identified in *Drosophila*, 3406 genes (24.5%) were identified to be directly associated with HP1a, while 10,489 genes (75.5%) are not associated with HP1a. (E and F) Metagene analysis of HP1a enrichment on genes. HP1a is enriched in the (E) promoter region 0.5-kb upstream of the TSS and in the (F) 3′ UTR region of the associated genes. (G) Some differentially regulated maternal effect genes are directly associated with HP1a. HP1a enrichment at each site was calculated as fold enrichment over mock ChIP conducted using mouse α-FLAG antibody. A total of six different classes of genes (regions) are shown. (a) Known HP1a-binding sites near transposable elements (*HeT-A* and *copia*); genes that are upregulated upon HP1a reduction, and are (b) directly associated with HP1a (*piwi* and *myo*) and (c) not associated with HP1a (*Sxl*, *sqd*, *nos*, *osk*, *Dip3*, *tkv*, and *qin*); genes that are downregulated upon HP1a reduction and are (d) directly associated with HP1a (*INCENP*, *aurB*, *AGO3*, and *Tudor-SN*) and (e) not associated with HP1a (*CycB3*, *cid*, *Su(var)3-7*, *Tdrd3*, and *Orc1*); and (f) known negative HP1a-binding sites (*Actin 5C* and *α-actinin*). Error bars indicate the mean Cq value ± SEM in three biological replicates. ChIP-seq, chromatin immunoprecipitation-sequencing; Chr, chromosome; TE, ; TSS, transcription start site; TTS, transcription termination site.

compact chromatin was associated with HP1a foci, while diffuse chromatin organization was observed where HP1a foci were absent (Figure 4E), supporting a direct role of maternal HP1a in establishing heterochromatin in the early embryo.

However, the disruption of overall nuclear organization is unlikely only due to direct HP1a participation (Figure 4), but also reflects the role of HP1a in regulating the transcription of maternal factors and pathways that are involved in nuclear organization, as well as the contribution of proper chromatin assembly to nuclear organization. In support of the above notion, our transcriptome analysis of HP1a-deficient stage 14 egg chambers revealed a broader impact of maternal HP1a in regulating factors that drive early embryogenesis. We identified 1360 maternal transcripts that were differentially affected upon HP1a reduction in the ovary. Among them, transcripts that are negatively regulated by HP1a include those involved in regulating neurogenesis, organ growth, germ cell development, and dorsal ventral pattern formation (Figure 5), all of which are processes that take place later in embryogenesis. These genes include *piwi*, *sqd*, *nos*, and *osk*. This suggests that HP1a is likely involved in preventing the expression of genes that promote germline development, and dorsal and ventral patterning, until the appropriate stage in embryogenesis. Many of the differentially expressed genes were also bound by HP1a, indicating a direct role of HP1a in regulating the transcription of these genes.

Genes that are positively regulated by HP1a include those involved in translation, mRNA splicing, and the regulation of mitosis (Figure 5), indicating that HP1a positively regulates genes that will promote the expressions of various maternal transcripts within the embryo, as well as those involved in regulating the early embryonic cycles. De Lucia *et al.* (2005) demonstrated that HP1a modulates the transcription of cell cycle regulators in a *Drosophila* embryonic cell line. Our study further provides *in vivo* evidence for the role of HP1a in activating the expression of cell cycle regulators. Many genes that are known to be essential for chromosome condensation, DNA replication, and mitosis, such as *Aurora B*, *INCENP*, *cid*, *CycB3*, and *Ago 3*, are positively regulated by HP1a. Thus, in addition to the reduction of maternal HP1a, these early embryos also inherit reduced amounts of cell cycle regulators, which would collectively contribute to the disruption of the nuclear structure.

Upon reducing the expression level of HP1a, a global change in histone modifications was observed in the late stage 14 egg chambers, further supporting the genome-wide role of HP1a in regulating transcription. Consistent with the known function of HP1a in heterochromatin maintenance, the silencing histone marks H3K9me3 and H3K27me3 were decreased when HP1a expression was reduced, whereas the H3K4me3-activating mark was increased. On the other hand, H4Ac, which is another activating histone mark, was greatly reduced upon HP1a deficiency, suggesting a role of HP1a in transcriptional activation via an H4Ac-related mechanism. Interestingly, H2Av, which is known to localize to heterochromatin and to help HP1a recruitment to the centromeric region, is increased upon reducing HP1a expression (Swaminathan *et al.* 2005), possibly reflecting an HP1a compensation mechanism. In addition, HP1a interacts with numerous binding partners, including histone methyltransferases, RNA pol II, and hnRNPs, all of which allow HP1a to participate in gene regulation (Piacentini *et al.* 2009; Bosch-Presegué *et al.* 2017). All these action mechanisms of HP1a might contribute to its function as a maternal regulator of early embryogenesis.

The role of maternal HP1a in regulating early *Drosophila* embryogenesis can be explored further. Maternal-to-zygotic transition occurs at cycle 14 in *Drosophila* embryos and zygotic HP1a protein is first detected at cycle 14. Thus, maternal HP1a is responsible for regulating zygotic transcription at the onset of maternal-to-zygotic transition. Identifying differentially expressed, newly synthesized zygotic transcripts in cycle 14 embryos with a reduced load of maternal HP1a would reveal zygotic genes that are regulated by maternal HP1a. Direct function of HP1a as well as those of the HP1a-regulated gene products in regulating mid- to late-stage *Drosophila* embryogenesis would reveal common and developmental stage-specific roles of HP1a.

## Acknowledgments

We thank the Lin laboratory members, especially Hongying Qi, for valuable comments and support; Thomas Kaufman for the centrosome antibody; the Iowa Hybridoma Bank for antibodies against lamin and HP1a; Lynn Cooley for the MTD-GAL4 flies and valuable comments; Sarah Elgin for the *Su(var)2-5*$^{04}$ flies; and the Bloomington *Drosophila* Stock Center and the Transgenic RNAi project for the RNAi flies. The transgenic fly generation, and the transcriptome and ChIP-seq analyses were supported by the National Institutes of Health (DP1 CA-174418) and a grant from the Mathers Foundation to H.L. We also thank Dr. Mei Zhong from the Yale Stem Cell Center Sequencing Core for carrying out the deep sequencing. The authors declare no conflict of interest.

Author contributions: H.L. and A.R.P. conceived and designed the project. A.R.P. conducted all experiments except: N.N. designed and contributed to generating transgenic fly lines, and Q.G. conducted immunoblot experiments in Figure 2A and Figure S4. N.L. conducted the bioinformatics analysis. A.R.P. and N.L. prepared the figures. A.R.P., N.L., and H.L. wrote the paper, and N.N. and Q.G. reviewed and edited the paper.

## Literature Cited

Ainsztein, A. M., S. E. Kandels-Lewis, A. M. Mackay, and W. C. Earnshaw, 1998 INCENP centromere and spindle targeting: identification of essential conserved motifs and involvement of heterochromatin protein HP1. J. Cell Biol. 143: 1763–1774. https://doi.org/10.1083/jcb.143.7.1763

Anders, S., and W. Huber, 2010 Differential expression analysis for sequence count data. Genome Biol. 11: R106. https://doi.org/10.1186/gb-2010-11-10-r106

Bannister, A. J., P. Zegerman, J. F. Partridge, E. A. Miska, J. O. Thomas *et al.*, 2001 Selective recognition of methylated lysine 9 on histone H3 by the HP1 chromo domain. Nature 410: 120–124. https://doi.org/10.1038/35065138

Bosch-Presegué, L., H. Raurell-Vila, J. K. Thackray, J. Gonzalez, C. Casal *et al.*, 2017 Mammalian HP1 isoforms have specific roles in heterochromatin structure and organization. Cell Rep. 21: 2048–2057. https://doi.org/10.1016/j.celrep.2017.10.092

Chakraborty, A., K. V. Prasanth, and S. G. Prasanth, 2014 Dynamic phosphorylation of HP1alpha regulates mitotic progression in human cells. Nat. Commun. 5: 3445. https://doi.org/10.1038/ncomms4445

Cryderman, D. E., S. K. Grade, Y. Li, L. Fanti, S. Pimpinelli *et al.*, 2005 Role of Drosophila HP1 in euchromatic gene expression. Dev. Dyn. 232: 767–774. https://doi.org/10.1002/dvdy.20310

De Lucia, F., J. Q. Ni, C. Vaillant, and F. L. Sun, 2005 HP1 modulates the transcription of cell-cycle regulators in Drosophila melanogaster. Nucleic Acids Res. 33: 2852–2858. https://doi.org/10.1093/nar/gki584

Edgar, B. A., and G. Schubiger, 1986 Parameters controlling transcriptional activation during early Drosophila development. Cell 44: 871–877. https://doi.org/10.1016/0092-8674(86)90009-7

Eissenberg, J. C., G. D. Morris, G. Reuter, and T. Hartnett, 1992 The heterochromatin-associated protein HP-1 is an essential protein in Drosophila with dosage-dependent effects on position-effect variegation. Genetics 131: 345–352.

Elgin, S. C., and G. Reuter, 2013 Position-effect variegation, heterochromatin formation, and gene silencing in Drosophila. Cold Spring Harb. Perspect. Biol. 5: a017780. https://doi.org/10.1101/cshperspect.a017780

Fischle, W., B. S. Tseng, H. L. Dormann, B. M. Ueberheide, B. A. Garcia *et al.*, 2005 Regulation of HP1-chromatin binding by histone H3 methylation and phosphorylation. Nature 438: 1116–1122. https://doi.org/10.1038/nature04219

Fleming, C. J., N. N. Yin, S. L. Riechers, G. Chu, and G. Y. Liu, 2011 High-resolution imaging of the intramolecular structure of indomethacin-carrying dendrimers by scanning tunneling microscopy. ACS Nano 5: 1685–1692. https://doi.org/10.1021/nn103609b

Foe, V. E., G. Odell, and B. Edgar, 1993 Mitosis and morphogenesis in the Drosophila embryo: point and counterpoint, pp. 149–300 in *The Development of Drosophila Melanogaster*, edited by M. Bate, and A. Martinez-Arias. Cold Spring Harbor Laboratory Press, Cold Spring Harbor, NY.

Greil, F., I. van der Kraan, J. Delrow, J. F. Smothers, E. de Wit *et al.*, 2003 Distinct HP1 and Su(var)3–9 complexes bind to sets of developmentally coexpressed genes depending on chromosomal location. Genes Dev. 17: 2825–2838. https://doi.org/10.1101/gad.281503

Gutzeit, H., and R. Koppa, 1982 Time-lapse film analysis of cytoplasmic streaming during late oogenesis of Drosophila. J. Embryol. Exp. Morphol. 67: 101–111.

Hirota, T., J. J. Lipp, B. H. Toh, and J. M. Peters, 2005 Histone H3 serine 10 phosphorylation by Aurora B causes HP1 dissociation from heterochromatin. Nature 438: 1176–1180. https://doi.org/10.1038/nature04254

Huang, X. A., H. Yin, S. Sweeney, D. Raha, M. Snyder *et al.*, 2013 A major epigenetic programming mechanism guided by piRNAs. Dev. Cell 24: 502–516. https://doi.org/10.1016/j.devcel.2013.01.023

Huang da, W., B. T. Sherman, and R. A. Lempicki, 2009 Systematic and integrative analysis of large gene lists using DAVID bioinformatics resources. Nat. Protoc. 4: 44–57. https://doi.org/10.1038/nprot.2008.211

James, T. C., and S. C. Elgin, 1986 Identification of a nonhistone chromosomal protein associated with heterochromatin in Drosophila melanogaster and its gene. Mol. Cell. Biol. 6: 3862–3872. https://doi.org/10.1128/MCB.6.11.3862

James, T. C., J. C. Eissenberg, C. Craig, V. Dietrich, A. Hobson *et al.*, 1989 Distribution patterns of HP1, a heterochromatin-associated nonhistone chromosomal protein of Drosophila. Eur. J. Cell Biol. 50: 170–180.

Kellum, R., and B. M. Alberts, 1995 Heterochromatin protein 1 is required for correct chromosome segregation in Drosophila embryos. J. Cell Sci. 108: 1419–1431.

Kellum, R., J. W. Raff, and B. M. Alberts, 1995 Heterochromatin protein 1 distribution during development and during the cell cycle in Drosophila embryos. J. Cell Sci. 108: 1407–1418.

Krzywinski, M., J. Schein, I. Birol, J. Connors, R. Gascoyne *et al.*, 2009 Circos: an information aesthetic for comparative genomics. Genome Res. 19: 1639–1645. https://doi.org/10.1101/gr.092759.109

Lachner, M., D. O'Carroll, S. Rea, K. Mechtler, and T. Jenuwein, 2001 Methylation of histone H3 lysine 9 creates a binding site for HP1 proteins. Nature 410: 116–120. https://doi.org/10.1038/35065132

Larson, A. G., D. Elnatan, M. M. Keenen, M. J. Trnka, J. B. Johnston *et al.*, 2017 Liquid droplet formation by HP1alpha suggests a role for phase separation in heterochromatin. Nature 547: 236–240. https://doi.org/10.1038/nature22822

Li, Y., J. R. Danzer, P. Alvarez, A. S. Belmont, and L. L. Wallrath, 2003 Effects of tethering HP1 to euchromatic regions of the Drosophila genome. Development 130: 1817–1824. https://doi.org/10.1242/dev.00405

Liao, Y., G. K. Smyth, and W. Shi, 2013 The subread aligner: fast, accurate and scalable read mapping by seed-and-vote. Nucleic Acids Res. 41: e108. https://doi.org/10.1093/nar/gkt214

Marlow, F. L., 2010 *Maternal Control of Development in Vertebrates: My Mother Made Me Do It!* Morgan & Claypool Life Sciences, San Rafael, CA.

Muller, H. R., and J. R. Tyler, 1930 The effect of the X-ray on the nodules of verruga peruana. J. Exp. Med. 51: 23–26. https://doi.org/10.1084/jem.51.1.23

Paro, R., and D. S. Hogness, 1991 The Polycomb protein shares a homologous domain with a heterochromatin-associated protein of Drosophila. Proc. Natl. Acad. Sci. USA 88: 263–267. https://doi.org/10.1073/pnas.88.1.263

Perkins, L. A., L. Holderbaum, R. Tao, Y. Hu, R. Sopko *et al.*, 2015 The Transgenic RNAi Project at Harvard Medical School: resources and validation. Genetics 201: 843–852. https://doi.org/10.1534/genetics.115.180208

Petrella, L. N., T. Smith-Leiker, and L. Cooley, 2007 The Ovhts polyprotein is cleaved to produce fusome and ring canal proteins required for Drosophila oogenesis. Development 134: 703–712. https://doi.org/10.1242/dev.02766

Piacentini, L., L. Fanti, M. Berloco, B. Perrini, and S. Pimpinelli, 2003 Heterochromatin protein 1 (HP1) is associated with induced gene expression in Drosophila euchromatin. J. Cell Biol. 161: 707–714. https://doi.org/10.1083/jcb.200303012

Piacentini, L., L. Fanti, R. Negri, V. Del Vescovo, A. Fatica *et al.*, 2009 Heterochromatin protein 1 (HP1a) positively regulates euchromatic gene expression through RNA transcript association and interaction with hnRNPs in Drosophila. PLoS Genet. 5: e1000670. https://doi.org/10.1371/journal.pgen.1000670

Richards, E. J., and S. C. Elgin, 2002 Epigenetic codes for heterochromatin formation and silencing: rounding up the usual suspects. Cell 108: 489–500. https://doi.org/10.1016/S0092-8674(02)00644-X

Ruppert, J. G., K. Samejima, M. Platani, O. Molina, H. Kimura *et al.*, 2018 HP1α targets the chromosomal passenger complex for

activation at heterochromatin before mitotic entry. EMBO J. 37: e97677. https://doi.org/10.15252/embj.201797677

Staller, M. V., D. Yan, S. Randklev, M. D. Bragdon, Z. B. Wunderlich *et al.*, 2013 Depleting gene activities in early Drosophila embryos with the "maternal-Gal4-shRNA" system. Genetics 193: 51–61. https://doi.org/10.1534/genetics.112.144915

Strom, A. R., A. V. Emelyanov, M. Mir, D. V. Fyodorov, X. Darzacq *et al.*, 2017 Phase separation drives heterochromatin domain formation. Nature 547: 241–245. https://doi.org/10.1038/nature22989

Su, T. T., 2007 Immunoblotting of proteins from single Drosophila embryos. CSH Protoc. 2007: pdb.prot4713. https://doi.org/10.1101/pdb.prot4713

Swaminathan, J., E. M. Baxter, and V. G. Corces, 2005 The role of histone H2Av variant replacement and histone H4 acetylation in the establishment of Drosophila heterochromatin. Genes Dev. 19: 65–76. https://doi.org/10.1101/gad.1259105

Vermaak, D., and H. S. Malik, 2009 Multiple roles for heterochromatin protein 1 genes in Drosophila. Annu. Rev. Genet. 43: 467–492. https://doi.org/10.1146/annurev-genet-102108-134802

Warecki, B., and W. Sullivan, 2018 Aurora B-mediated exclusion of HP1a from late-segregating chromatin prevents formation of micronuclei. bioRxiv. Available at: https://www.biorxiv.org/content/early/2018/02/21/268912. https://doi.org/10.1101/268912

Xie, H., C. Peng, J. Huang, B. E. Li, W. Kim *et al.*, 2016 Chronic myelogenous leukemia- initiating cells require polycomb group protein EZH2. Cancer Discov. 6: 1237–1247. https://doi.org/10.1158/2159-8290.CD-15-1439

Yan, D., R. A. Neumuller, M. Buckner, K. Ayers, H. Li *et al.*, 2014 A regulatory network of Drosophila germline stem cell self-renewal. Dev. Cell 28: 459–473. https://doi.org/10.1016/j.devcel.2014.01.020

Yin, H., S. Sweeney, D. Raha, M. Snyder, and H. Lin, 2011 A high-resolution whole-genome map of key chromatin modifications in the adult Drosophila melanogaster. PLoS Genet. 7: e1002380. https://doi.org/10.1371/journal.pgen.1002380

*Communicating editor: B. Calvi*